Recursive Bayesian filtering for multitarget track-before-detect in passive radars

Frederic Lehmann

Abstract

This paper presents a Bayesian algorithm for joint detection and tracking in a multitarget setting. Raw measurements are processed using the track-before-detect framework. We first establish a Bayesian recursion, which propagates a probability of target existence along with a target state probability density per delay/Doppler bin. In order to handle the nonlinearity of the observation model obtained for OFDM-based passive radar, a suitable Gaussian mixture implementation is proposed.

Index Terms

Bayesian filtering, track-before-detect, multitarget tracking, Gaussian sum filtering, passive radar, OFDM signals.

I. Introduction

During the last two decades, there has been a renewed interest in passive radar systems for civilian and military applications [1]-[3]. We will consider a bistatic configuration, where the antennas used for transmission and reception are located at different positions. The main characteristic of passive radars is that they use commercial broadcasters as illuminators of opportunity. Among the advantages, the detection and localization of targets is covert, continuous and also inexpensive, since the transmitter needs neither frequency allocation nor extra hardware. However, since the transmitted signal is not under control, existing systems relying on analog TV or FM transmissions suffer from large and time-varying sidelobes in the ambiguity function [4]. Recently, passive surveillance radars based on digital audio broadcasting (DAB) [5] or digital video broadcasting (DVB) [6] have been investigated [7]-[9]. These systems rely on base stations transmitting COFDM (Coded Orthogonal Frequency Division Multiplexing) signals with good bistatic range resolution and lower sidelobes. Moreover, the presence of a powerful error correcting code enables to reconstruct a quasi error free copy of the transmitted signal at the reference antenna for the purpose of crosscorrelation with the signal at the measurement antenna. This operation, also called matched filtering, is used to generate raw measurements.

In this paper, we consider multiple target detection and tracking, which is a challenging problem due to the presence of an unknown and varying number of moving targets in the environment.

Classical methods generate so-called plots by thresholding the raw measurements, which incurs missed detections and false alarms due to the presence of clutter. The data association problem, which stems from the unknown association of plots with targets and clutter, must be solved. Traditional solutions include the multiple hypotheses tracker (MHT) [10], which propagates

The author is with INSTITUT TELECOM, TELECOM SudParis, departement CITI, UMR-CNRS 5157, 91011 Evry Cedex, France (e-mail: frederic.lehmann@it-sudparis.eu).
Phone: (+33) 1 60 76 46 33. Fax: (+33) 1 60 76 44 33
Manuscript received February 14, 2011; revised July 6, 2011.

a number of association hypotheses in time, the joint probabilistic data association filter (JPDAF) [11], which updates each track with plots weighted by the corresponding association probabilities and the probability hypothesis density filter (PHDF) [12], which propagates the first-order statistic of the random finite set of the targets in time.

In all the aforementioned techniques, the thresholding stage generating the plots incurs a loss of information, so these methods may be far from optimal for very low signal-to-noise ratio (SNR) targets. A well-known alternative, referred to as track-before-detect (TBD), processes the raw measurements without thresholding. This technique has essentially two advantages. Firstly, TBD circumvents the data association problem. Secondly, information in a track can now benefit from long coherent integration over time, so that the decision can be postponed until the end of the processing chain. Therefore a target, which is too weak to generate detections after classical thresholding of raw measurements, could still be detected using TBD. In the batch method proposed in [13]-[16], TBD is implemented via dynamic programming for single target detection. A generalization to multi-target environments is provided in [17]. The main drawback of the batch method is that the state-space needs to be discretized over a discrete grid. Therefore the root mean square errror (RMSE) for any target is approximately equal to half the grid bin size, irrespective of the target's actual SNR. Recursive Bayesian particle-based solutions have also been proposed in [18]-[19] for a single target scenario. Since a continuous-valued state-space is used, the RMSE decreases with the target SNR. The main interest of these methods is the introduction of a target existence variable, whose *a posteriori* probability is estimated jointly with the target state. An extension to multitarget scenarios, which estimates recursively the number of targets along with their states, was presented in [20]. This particle-based method jointly estimates the targets by augmenting the dimension of the state-space. An obvious limitation is that this approach suffers from the curse of dimensionality [21] when the number of targets grows.

In this paper, we introduce a recursive Bayesian TBD solution to the multitarget detection and tracking problem. The proposed structure is inherited from classical radar detection theory, where the delay/Doppler space is divided into regularly spaced intervals. The size of a delay (resp. Doppler) bin corresponds to the delay (resp. Doppler) resolution of the radar system [22]. Implicitly, we assume as in classical radar detection, that only one target can be resolved within a single delay/Doppler bin. In [19], single target TBD was achieved by computing recursively the probability of target existence and the probability distribution function (pdf) of the target state, conditioned on target existence. In order to obtain a multitarget detection and tracking algorithm, we generalize this idea so that each delay/Doppler bin is associated with a probability of target existence and a target state pdf, conditioned on target existence. Since the observation model is a nonlinear function of the target state, the desired Bayesian recursion requires some form of approximation, since it involves multiplications and integrals that cannot be expressed in closed form. Unlike the computationally intensive particle filtering solution retained in [19], we use a single

Gaussian per delay/Doppler bin to propagate the target state pdf in time, in the same spirit as the Gaussian sum filter [23]. The resulting algorithm performs a surveillance of the entire state-space, since at each instant of time, each delay/Doppler bin estimates the probability that a target is present (which is akin to fixed grid target detection) along with the corresponding target state pdf (which is akin to continuous-valued state tracking). Therefore, our mixed discrete-continuous state-space formulation retains the best of both worlds.

Throughout the paper, bold letters indicate vectors and matrices, while $\mathbf{I}_m$ denotes the $m \times m$ identity matrix and $\mathbf{0}_{n\times m}$ the $n \times m$ all-zero matrix. A diagonal matrix, whose diagonal entries are stored in vector $\mathbf{a}$ and whose off-diagonal entries are zero, is denoted by $\mathrm{diag}\{\mathbf{a}\}$. $\mathcal{N}(\mathbf{x} : \mathbf{m}, \mathbf{P})$ denotes a Gaussian distribution of the variable $\mathbf{x}$, with mean $\mathbf{m}$ and covariance matrix $\mathbf{P}$. $\mathrm{sinc}(.)$ (resp. $\Pi_a(.)$) denote the sinus cardinal function (resp. the rectangle function that is zero outside the interval $[-a/2, a/2]$ and unity inside). The dot product of two vectors $\mathbf{u} = [u_1, u_2, \ldots, u_n]^T$ and $\mathbf{v} = [v_1, v_2, \ldots, v_n]^T$ is defined as $\mathbf{u}.\mathbf{v} = \sum_{i=1}^{n} u_i v_i$.

This paper is organized as follows. First, Sec. II describes the system model adopted for passive radar using OFDM signals. In Sec. III, the problem is cast into a mixed discrete-continuous state-space formulation. In Sec. IV, we introduce our Bayesian recursion for TBD mutitarget detection and tracking. In Sec. V, we propose a tractable Gaussian mixture implementation. Sec. VI describes several benchmark algorithms, adapted to the targeted passive radar application. Finally, in Sec. VII, the performances of the proposed algorithm are assessed through numerical simulations and compared with existing methods.

II. Passive Radar System Model

In Sec. II-A, we model the signal at the receive antenna, assuming that the transmitter is an illuminator of opportunity sending a COFDM signal. Matched filtering is discussed in Sec. II-B. Then, in Sec. II-C, we propose an apodization technique to reduce the sidelobe level at the matched filter output.

A. Signal Model

Figure 1: About here.

In passive radar systems, the transmit and receive antennas are not collocated, as illustrated by Fig. 1. The illuminator of opportunity sends a continuous COFDM signal of bandwidth B, whose complex baseband equivalent signal is denoted by $s(t)$. At the receive antenna, the contribution of a moving target has the form [24]

$$s_r(t) = A(t)e^{j\theta(t)}e^{j2\pi\nu(t)t}s(t - \tau(t)) + w(t). \tag{1}$$

The time-dependent parameters A, θ, ν and τ denote the amplitude, the phase, the Doppler frequency and the propagation delay, respectively. For simplicity, the contribution of clutter and ambient noise is modeled as a zero-mean complex additive

white Gaussian noise (AWGN) $w(t)$, with variance σ^2. Let $\mathbf{x}_e$, $\mathbf{x}_r$ and $\mathbf{x}(t)$ denote the position of the emitter, receiver and target in a 3D cartesian coordinate system. Let $\mathbf{v}(t)$ denote the target velocity vector. Let f_c be the carrier frequency of the COFDM signal and c the speed of light, then $\tau(t)$ and $\nu(t)$ can be expressed as [1]

$$\tau(t) = \frac{||\mathbf{x}(t) - \mathbf{x}_e|| + ||\mathbf{x}(t) - \mathbf{x}_r||}{c}$$
$$\nu(t) = \frac{f_c}{c}\mathbf{v}(t).\left(\frac{\mathbf{x}(t) - \mathbf{x}_e}{||\mathbf{x}(t) - \mathbf{x}_e||} + \frac{\mathbf{x}(t) - \mathbf{x}_r}{||\mathbf{x}(t) - \mathbf{x}_r||}\right).$$

We make the following assumptions:

Assumption 2.1: If multiple targets are present in the environment, their contributions add up in (1).

Assumption 2.2: The contribution of the direct path and ground clutter is below the noise floor using the methods suggested in [3], namely physical shielding, Doppler processing, high gain antennas, sidelobe cancellation, adaptive beamforming or adaptive filtering.

Assumption 2.3: Assuming perfect knowledge of the propagation delay of the direct path between the emitter and the receiver, the receiver has a reference channel able to recover $s(t)$ perfectly, since quasi error free detection is made possible for COFDM signals with powerful error correcting codes [5]-[6].

B. Matched filtering

Coherent integration is performed by cross correlating the received signal with the reference signal $s_{ref}(t)$, shifted in delay and frequency. This operation is called matched filtering and has the property of maximizing the peak SNR [22]. To cancel unwanted side-peaks, the reference signal $s_{ref}(t)$ must be chosen as the transmitted signal $s(t)$ with the following modifications [9]: guard interval blanking, pilot carriers equalization for intra-symbol peak mitigation and pilot carriers filtering for intersymbol peak mitigation.

Let T denote the integration time. Assuming that T is sufficiently small, the signal parameters A, θ, ν and τ can be considered as constant during each integration window. During the k-th integration window, the output of the matched filter corresponding to a delay shift t and frequency shift f is given by

$$r_k(t,f) = \frac{1}{T}\int_{kT-T/2}^{(k+1)T-T/2} s_r(\theta)s_{ref}(\theta - t)^* e^{-j2\pi f\theta}d\theta \tag{2}$$

Injecting (1) into (2), we obtain

$$\begin{aligned} r_k(t,f) = {} & Ae^{j\theta} \\ & \times \frac{1}{T}\int_{kT-T/2}^{(k+1)T-T/2} s(\theta - \tau)s_{ref}(\theta - t)^* e^{-j2\pi(f-\nu)\theta}d\theta \\ & + z_k(t,f) \end{aligned} \tag{3}$$

where $z_k(t,f)$ is the noise term

$$z_k(t,f) = \frac{1}{T} \int_{kT-T/2}^{(k+1)T-T/2} w(\theta) s_{ref}(\theta - t)^* e^{-j2\pi f\theta} d\theta. \tag{4}$$

Using the change of variable $u = \theta - t - kT$, (3) becomes

$$\begin{aligned} r_k(t,f) &= Ae^{j\theta} e^{-j2\pi(f-\nu)(t+kT)} \\ &\times \frac{1}{T} \int_{-T/2-t}^{T/2-t} s(u+kT+t-\tau) s_{ref}(u+kT)^* e^{-j2\pi(f-\nu)u} du \\ &+ z_k(t,f) \end{aligned} \tag{5}$$

Define the generalized ambiguity function (GAF) as

$$\begin{aligned} \chi(t,f) &= \frac{1}{T} \int_{-T/2}^{T/2} s(u+t) s_{ref}(u)^* e^{-j2\pi f u} du \\ &\approx L \operatorname{sinc}(Bt) \times \operatorname{sinc}(Tf). \end{aligned} \tag{6}$$

where the approximation, which is valid for T sufficiently large, is a consequence of the rectangular spectrum of the OFDM signal [25]. The parameter $0 < L < 1$ is the power loss factor induced by guard interval and pilot carriers modification [9]. Again, if T is sufficiently large, (5) can be written as

$$r_k(t,f) = Ae^{j\theta} e^{-j2\pi(f-\nu)(t+kT)} \chi(t-\tau, f-\nu) + z_k(t,f). \tag{7}$$

The noise term $z_k(t,f)$ is Gaussian distributed and has the following first and second-order statistics (see Appendix E)

$$\begin{aligned} E[z_k(t,f)] &= 0 \\ E[z_k(t,f) z_k(t-\theta, f-\varphi)^*] &= \frac{\sigma^2}{T} \chi(\theta,\varphi) e^{-j2\pi\varphi(t+kT)}. \end{aligned} \tag{8}$$

Remark 2.4: According to (6), the correlation of the Gaussian noise in the second equation of (8) is significant only for $|\theta| < 1/2B$ and $|\varphi| < 1/2T$.

C. Reduction of sidelobes

The sine cardinal envelope of the matched filter output in not acceptable, since sidelobes can be mistaken for targets or mask nearby weak targets [22]. Various apodization techniques have been proposed to suppress the sidelobes. Linear sidelobe reduction techniques are weighting functions applied to the matched filter output in the time domain [22]. These techniques are simple to implement, but they cause an increase in the mainlobe width. Therefore, it is preferable to use nonlinear apodization. We use the standard spatially variant apodization (SVA) technique [26], originally applied to in-phase (I) and quadrature (Q) components of complex synthetic aperture radar (SAR) pixels. In our application, the SAR pixels are replaced by sampled matched filter outputs. To achieve proper sidelobe cancellation with SVA, the sampling frequency on the delay and frequency shift axis must be settled to a multiple of the Nyquist frequency [27]. That is, the matched filter output (7) is sampled at delay

shifts and frequency shifts of the form

$$\begin{aligned} t_i &= t_0 + i\frac{1}{R_t B}, \quad i = 0, \ldots, I \\ f_j &= f_0 + j\frac{1}{R_f T}, \quad j = 0, \ldots, J \end{aligned} \tag{9}$$

where $R_t \in \{1, 2\}$ (resp. $R_f \in \{1, 2\}$) represents the integer delay (resp. frequency) shift oversampling factor. Note that an efficient implementation of the discretized matched filter output using the fast Fourier transform (FFT) has appeared in [24], where MUSIC or Basis Poursuit approaches where suggested to remove the sidelobes of the targets. More precisely, we use the I&Q jointly SVA (also called Type 3 in [27]), since it was shown in [28] that this version of SVA introduces the smallest distorsion on the noise pdf. Consequently, applying sampling and I&Q jointly SVA to (7), we obtain the following matrix of noisy observations

$$y_k^{i,j} = Ae^{j\theta} e^{-j2\pi(f_j - \nu)(t_i + kT)} \tilde{\chi}(t_i - \tau, f_j - \nu) + n_k^{i,j}, \tag{10}$$

for $i = 0, \ldots, I$ and $j = 0, \ldots, J$. Assuming that the remaining sidelobe contributions after apodization are under the noise floor, the apodized GAF becomes

$$\tilde{\chi}(t, f) = L\,\mathrm{sinc}(Bt)\Pi_{2/B}(t) \times \mathrm{sinc}(Tf)\Pi_{2/T}(t). \tag{11}$$

Let $\mathbf{y}_k = \{y_k^{i,j}\}$ for $0 \leq i \leq I$, $0 \leq j \leq J$ be the matrix of noisy observations at instant k, the collection of past and present observations will be denoted by $\mathbf{y}_{1:k} = \{\mathbf{y}_1, \ldots, \mathbf{y}_k\}$.

Remark 2.5: We were able to verify experimentally that the noise terms $n_k^{i,j}$, for $i = 0, \ldots, I$ and $j = 0, \ldots, J$ can be assimilated to a zero-mean Gaussian process, with only slighlty different variance and correlation properties with respect to the original noise before SVA.

Remark 2.6: The delay and frequency resolution are independently determined by the bandwidth B and the integration time T, respectively. Moreover, thanks to SVA apodization, the range and Doppler ambiguities have been removed.

III. Discrete-time dynamical system model

Since our objective is to perform Bayesian multitarget detection and tracking, we introduce a suitable state-space representation (see Sec. III-A). In each bin (to be defined), a discrete-valued random variable models the presence or absence of a target and a continuous-valued random variable models the kinematic state of the target.

Then, we will turn our attention to the dynamics of the proposed model by considering two cases. In the first case, we study the dynamics of the proposed system within a given bin (see Sec. III-B). This is the standard behavior, since when a target appears in a given bin, it will typically remain in that bin for a number of consecutive time steps. Then, we treat the case when a target crosses the boundaries of a bin (see Sec. III-C). Indeed, proper boundary conditions must be provided, so that that a target crossing bin boundaries is not lost.

A. State-space representation

Figure 2: About here.

The discretization of the delay and frequency shifts in (9) defines an implicit partition of the delay/frequency plane into bins, as illustrated by Fig. 2. We define the i-th delay bin as the interval $[t_{i-1}, t_i]$, for $i = 1, \ldots, I$. Similarly, define the j-th frequency bin as the interval $[f_{j-1}, f_j]$, for $j = 1, \ldots, J$. The delay/frequency bin (i, j) is then defined as $[t_{i-1}, t_i] \times [f_{j-1}, f_j]$. We associate a target existence variable $e_k^{i,j}$ to the delay/frequency bin (i, j). At the discrete instant k, $e_k^{i,j} = 0$ (resp. $e_k^{i,j} = 1$) corresponds to the absence (resp. presence) of a a target in bin (i, j). We note $P_b^{i,j}$ (resp. $P_d^{i,j}$) the prior probability of target birth (resp. death) in bin (i, j).

We now turn our attention to the target's kinematic state. Assume the presence of a point target in bin (i, j), with delay τ_k, Doppler frequency ν_k and Doppler rate ζ_k during the k-th integration window. After SVA apodization, the matched filter output response to a single target corresponds to a thumbtack ambiguity diagram [22]. Therefore the only significant radar signal returns corresponding to the presence of a target in bin (i, j) are $y_k^{i-1,j-1}$, $y_k^{i,j-1}$, $y_k^{i-1,j}$ and $y_k^{i,j}$. Consider the four complex SVA outputs in (10) $y_k^{i-1,j-1}$, $y_k^{i,j-1}$, $y_k^{i-1,j}$ and $y_k^{i,j}$ and let us ignore the noise contribution for the moment. According to (10), $y_k^{i-1,j-1}$, $y_k^{i,j-1}$ correspond to the same frequency shift sample f_{j-1}, and the phase rotation between them is negligible, considering that $1/R_t B \ll 1$ for OFDM signals. We let $a_k^I + j a_k^Q$ be the common complex amplitude of $y_k^{i-1,j-1}$ and $y_k^{i,j-1}$. With the same reasoning, we let $b_k^I + j b_k^Q$ be the common complex amplitude of $y_k^{i-1,j}$ and $y_k^{i,j}$. Collecting all these variables, we obtain the kinematic state vector $\mathbf{x}_k = [a_k^I, a_k^Q, b_k^I, b_k^Q, \tau_k, \nu_k, \zeta_k]^T$.

B. Intra-bin dynamics

Considering that the Doppler frequency is proportional to the first-order derivative of the delay and using a constant acceleration model, the dynamics of the target, at the discrete time instant k, are described by

$$\begin{cases} \tau_k = \tau_{k-1} - \nu_{k-1} \frac{T}{f_c} \\ \nu_k = \nu_{k-1} + \zeta_{k-1} T \\ \zeta_k = \zeta_{k-1} \end{cases} \tag{12}$$

Using the dynamical model for the complex amplitude introduced in [29], we obtain

$$\begin{cases} a_k^I = \cos\left[2\pi(\nu_{k-1} - f_{j-1})T\right] a_{k-1}^I - \sin\left[2\pi(\nu_{k-1} - f_{j-1})T\right] a_{k-1}^Q \\ a_k^Q = \sin\left[2\pi(\nu_{k-1} - f_{j-1})T\right] a_{k-1}^I + \cos\left[2\pi(\nu_{k-1} - f_{j-1})T\right] a_{k-1}^Q \\ b_k^I = \cos\left[2\pi(\nu_{k-1} - f_j)T\right] b_{k-1}^I - \sin\left[2\pi(\nu_{k-1} - f_j)T\right] b_{k-1}^Q \\ b_k^Q = \sin\left[2\pi(\nu_{k-1} - f_j)T\right] b_{k-1}^I + \cos\left[2\pi(\nu_{k-1} - f_j)T\right] b_{k-1}^Q \end{cases} \tag{13}$$

(12) and (13) can be written as a discrete-time process equation

$$\mathbf{x}_k = f(\mathbf{x}_{k-1}) + \mathbf{u}_k, \tag{14}$$

where the process noise $\mathbf{u}_k \sim \mathcal{N}(\mathbf{0}_{7\times 1}, \mathbf{Q})$ accounts for unmodeled perturbations and is assumed independent of the observation noise. Therefore, for the most common target behavior, that is when a target continues to exist in bin (i, j) for two consecutive

time instants

$$p(\mathbf{x}_k|\mathbf{x}_{k-1}, e_k^{i,j}=1, e_{k-1}^{i,j}=1) = \mathcal{N}\left(\mathbf{x}_k : f(\mathbf{x}_{k-1}), \mathbf{Q}\right) \tag{15}$$

A kinematic state birth pdf can be defined in a similar way as

$$p(\mathbf{x}_k|e_k^{i,j}=1, e_{k-1}^{i,j}=0) = \mathcal{N}\left(\mathbf{x}_k : \mathbf{x}_b^{i,j}, \mathbf{P}_b^{i,j}\right), \tag{16}$$

where the mean

$$\mathbf{x}_b^{i,j} = [0,0,0,0,(t_{i-1}+t_i)/2, (f_{j-1}+f_j)/2, 0]^T$$

is located at the middle of a bin (i,j) and the covariance matrix

$$\mathbf{P}_b^{i,j} = \mathrm{diag}\{[\sigma_a^2, \sigma_a^2, \sigma_a^2, \sigma_a^2, ((t_i - t_{i-1})/10)^2, ((f_j - f_{j-1})/2)^2, \sigma_\zeta^2]\}$$

accounts for the initial uncertainty on the state variables within bin (i,j). In particular, σ_a^2 and σ_ζ^2 are related to the dynamic range of the target amplitude and of the Doppler rate, respectively.

C. Inter-bin dynamics

We first introduce a few useful notations. Let $N(i,j) = \{(i,j),(i-1,j),(i+1,j),(i,j-1),(i,j+1)\}$ be the set containing (i,j) and the first-order neighborhood of (i,j). Since a target can migrate from time to time from a bin $(m,n) \in N(i,j)\setminus(i,j)$ to bin (i,j), boundary conditions must be defined for the dynamics.

We begin with the definition of transition probabilities for the discrete-valued target existence variable. Let $P(i,j|m,n,\mathbf{y}_{1:k-1})$ be the probability that a target present in bin $(m,n) \in N(i,j) \setminus (i,j)$ at instant $k-1$, travels to bin (i,j) at instant k, given $\mathbf{y}_{1:k-1}$ and given that it does not die out. For simplicity, we propose an expression which depends only on $\hat{\tau}_{k-1|k-1}^{m,n}$ and $\hat{\nu}_{k-1|k-1}^{m,n}$, which are respectively the delay and Doppler estimate, conditional on a target existence in bin (m,n) and on all the observations seen so far $\mathbf{y}_{1:k-1}$. For a frequency bin crossing, we choose

$$\begin{aligned} P(i,j|i,j-1,\mathbf{y}_{1:k-1}) &= \exp\left(-\alpha_\nu \left|\hat{\nu}_{k-1|k-1}^{i,j-1} - f_{j-1}\right|^2\right) \\ P(i,j|i,j+1,\mathbf{y}_{1:k-1}) &= \exp\left(-\alpha_\nu \left|\hat{\nu}_{k-1|k-1}^{i,j+1} - f_{j}\right|^2\right) \end{aligned} \tag{17}$$

where α_ν is a real parameter of choice. The proposed expression has the desirable property that the transition probability is close to 1 when $\hat{\nu}_{k-1|k-1}^{i,j\pm1}$ approaches a frequency bin boundary and vanishes exponentially otherwise. Similarly, delay bin transition probabilities have the form

$$\begin{aligned} P(i,j|i-1,j,\mathbf{y}_{1:k-1}) &= \exp\left(-\alpha_\tau \left|\hat{\tau}_{k-1|k-1}^{i-1,j} - t_{i-1}\right|^2\right) \\ P(i,j|i+1,j,\mathbf{y}_{1:k-1}) &= \exp\left(-\alpha_\tau \left|\hat{\tau}_{k-1|k-1}^{i+1,j} - t_{i}\right|^2\right). \end{aligned} \tag{18}$$

On the contrary, $P(i,j|i,j,\mathbf{y}_{1:k-1})$, the probability that a target present in bin (i,j) at instant $k-1$ remains in bin (i,j) at instant k, given $\mathbf{y}_{1:k-1}$ and given that it does not die out, should be close to one far from the boundaries of bin (i,j) and

vanish exponentially in the vicinity of the boundaries. Thus we can use

$$P(i,j|i,j,\mathbf{y}_{1:k-1}) = 1 - \max\Bigg\{ \exp\left(-\alpha_\nu \left|\hat{\nu}^{i,j}_{k-1|k-1} - f_{j-1}\right|^2\right) + \exp\left(-\alpha_\nu \left|\hat{\nu}^{i,j}_{k-1|k-1} - f_j\right|^2\right), \exp\left(-\alpha_\tau \left|\hat{\tau}^{i,j}_{k-1|k-1} - t_{i-1}\right|^2\right) + \exp\left(-\alpha_\tau \left|\hat{\tau}^{i,j}_{k-1|k-1} - t_i\right|^2\right)\Bigg\}. \tag{19}$$

According to the discussion on complex amplitudes at the end of Sec. III-A, the kinematic state transition pdf for a delay bin transition needs no modification with respect to (15)

$$\begin{aligned} &p(\mathbf{x}_k|\mathbf{x}_{k-1}, e^{i,j}_k = 1, e^{i-1,j}_{k-1} = 1) \\ &= p(\mathbf{x}_k|\mathbf{x}_{k-1}, e^{i,j}_k = 1, e^{i+1,j}_{k-1} = 1) = \mathcal{N}\left(\mathbf{x}_k : f(\mathbf{x}_{k-1}), \mathbf{Q}\right). \end{aligned} \tag{20}$$

However, for a frequency bin transition, the kinematic state transition pdf needs a slight modification, as indicated in Appendix A, to take into account the occurrence of a sharp phase jump.

D. Observation likelihood

From the discussion in Sec. III-A, the likelihood of the noisy observations considered for an existing point target in bin (i,j), conditioned on $\mathbf{x}_k$ can be written as

$$\begin{aligned} &p\left(y^{i-1,j-1}_k, y^{i,j-1}_k, y^{i-1,j}_k, y^{i,j}_k | e^{i,j}_k = 1, \mathbf{x}_k\right) \\ &= \mathcal{N}\left(\mathbf{y}^{i,j}_k : h^{i,j}(\mathbf{x}_k), \mathbf{R}\right), \end{aligned} \tag{21}$$

where

$$\mathbf{y}^{i,j}_k = \begin{bmatrix} \mathrm{Re}(y^{i-1,j-1}_k) \\ \mathrm{Im}(y^{i-1,j-1}_k) \\ \mathrm{Re}(y^{i,j-1}_k) \\ \mathrm{Im}(y^{i,j-1}_k) \\ \mathrm{Re}(y^{i-1,j}_k) \\ \mathrm{Im}(y^{i-1,j}_k) \\ \mathrm{Re}(y^{i,j}_k) \\ \mathrm{Im}(y^{i,j}_k) \end{bmatrix}$$

is the vector of real observations associated with bin (i,j). The observation noise covariance matrix $\mathbf{R}$ and the nonlinear observation function $h^{i,j}(.)$ are derived from (10). Namely, the observation function has the form

$$h^{i,j}(\mathbf{x}_k) = \begin{bmatrix} a^I_k \tilde{\chi}(t_{i-1} - \tau_k, f_{j-1} - \nu_k) \\ a^Q_k \tilde{\chi}(t_{i-1} - \tau_k, f_{j-1} - \nu_k) \\ a^I_k \tilde{\chi}(t_i - \tau_k, f_{j-1} - \nu_k) \\ a^Q_k \tilde{\chi}(t_i - \tau_k, f_{j-1} - \nu_k) \\ b^I_k \tilde{\chi}(t_{i-1} - \tau_k, f_j - \nu_k) \\ b^Q_k \tilde{\chi}(t_{i-1} - \tau_k, f_j - \nu_k) \\ b^I_k \tilde{\chi}(t_i - \tau_k, f_j - \nu_k) \\ b^Q_k \tilde{\chi}(t_i - \tau_k, f_j - \nu_k) \end{bmatrix}. \tag{22}$$

Similarly, we have

$$\begin{aligned} &p\left(y^{i-1,j-1}_k, y^{i,j-1}_k, y^{i-1,j}_k, y^{i,j}_k | e^{i,j}_k = 0\right) \\ &= \mathcal{N}\left(\mathbf{y}^{i,j}_k : \mathbf{0}_{8\times 1}, \mathbf{R}\right). \end{aligned} \tag{23}$$

Remark 3.1: The covariance matrix $\mathbf{R}$ is obtained straightforwardly from (8), if one assumes that SVA apodization has a negligible impact on the noise statistics. Alternatively, one can estimate the covariance matrix using the technique proposed in [15].

IV. Bayesian recursion for TBD multitarget detection and tracking

Our objective is to perform a global surveillance of the entire state-space without omission, at each instant of time. To achieve this, we propose to estimate the probability that a target is present (which is akin to target detection) along with the corresponding target kinematic state pdf (which is akin to target tracking) in each delay/frequency bin. Since Bayesian filtering is of interest in the present paper, we must calculate the *a posteriori* target existence probability, $P(e_k^{i,j} = 1|\mathbf{y}_{1:k})$, along with the pdf of an existing target's kinematic state $p(\mathbf{x}_k|e_k^{i,j} = 1, \mathbf{y}_{1:k})$, for each bin (i, j). From an implementation point of view, it is desirable to derive this filter in a recursive form. Sec. IV-A shows how to propagate the *a posteriori* target existence probability in time for each bin. Similarly, Sec. IV-B shows how to propagate the *a posteriori* pdf of an existing target's kinematic state in time for each bin. The issues of target detection and post-processing are discussed in Sec. IV-C and IV-D, respectively. Fig. 3 illustrates the complete TBD multitarget detection and tracking processing chain.

Figure 3: About here.

To derive the desired recursions we also need two simplifying assumptions:

Assumption 4.1: At most one target can be located in a given bin.

Assumption 4.2: A target present in bin (i, j) at instant $k - 1$, has either died out or is surviving in one of the bins $(m, n) \in N(i, j)$ at instant k.

Considering the system model of Sec. II, assumption (4.1) is substantiated by the fact that the size of a bin corresponds to the delay/frequency resolution of the radar system. Assumption (4.2) is justified by the limited speed of the targets, which cannot instantly travel through multiple delay/frequency bins.

A. Target existence probability

Under assumptions (4.1) and (4.2), the predicted target existence probability in bin (i, j) can be expanded over the presence of targets in bins $(m, n) \in N(i, j)$ at the previous time instant and the birth of a target in bin (i, j) at the current time instant

$$\begin{aligned} & P(e_k^{i,j} = 1|\mathbf{y}_{1:k-1}) \\ & = P(e_k^{i,j} = 1, e_{k-1}^{i,j} = 0|\mathbf{y}_{1:k-1}) + \\ & \quad \sum_{(m,n)\in\mathcal{N}(i,j)} P(e_k^{i,j} = 1, e_{k-1}^{m,n} = 1|\mathbf{y}_{1:k-1}) \\ & = P_b^{i,j} P(e_{k-1}^{i,j} = 0|\mathbf{y}_{1:k-1}) + \\ & \quad \sum_{(m,n)\in\mathcal{N}(i,j)} P(i, j|m, n, \mathbf{y}_{1:k-1})(1 - P_d^{m,n}) P(e_{k-1}^{m,n} = 1|\mathbf{y}_{1:k-1}) \end{aligned} \tag{24}$$

The birth, death and bin transition probabilities $P_b^{i,j}$, $P_d^{m,n}$ and $P(i,j|m,n,\mathbf{y}_{1:k-1})$, for $(m,n) \in N(i,j)$ have been defined previously in Sec. III.

The Bayesian correction step proceeds as follows

$$\begin{aligned} P(e_k^{i,j}=1|\mathbf{y}_{1:k}) \approx & \frac{p(y_k^{i-1,j-1}, y_k^{i,j-1}, y_k^{i-1,j}, y_k^{i,j}|e_k^{i,j}=1, \mathbf{y}_{1:k-1})}{p(y_k^{i-1,j-1}, y_k^{i,j-1}, y_k^{i-1,j}, y_k^{i,j}|\mathbf{y}_{1:k-1})} \\ & \times P(e_k^{i,j}=1|\mathbf{y}_{1:k-1}). \end{aligned} \tag{25}$$

As explained in Appendix B, this formula, although not exact, leads to a tractable solution. We also provide a justification of this approximate Bayesian correction step, relying on the apodization introduced in Sec. II-C.

The numerator in the first line of the right-hand side (RHS) of (25) can be evaluated by marginalizing out the kinematic state

$$\begin{aligned} & p(y_k^{i-1,j-1}, y_k^{i,j-1}, y_k^{i-1,j}, y_k^{i,j}|e_k^{i,j}=1, \mathbf{y}_{1:k-1}) \\ & = \int p(y_k^{i-1,j-1}, y_k^{i,j-1}, y_k^{i-1,j}, y_k^{i,j}, \mathbf{x}_k|e_k^{i,j}=1, \mathbf{y}_{1:k-1}) d\mathbf{x}_k. \end{aligned}$$

Applying Bayes's rule, we obtain

$$\begin{aligned} & p(y_k^{i-1,j-1}, y_k^{i,j-1}, y_k^{i-1,j}, y_k^{i,j}|e_k^{i,j}=1, \mathbf{y}_{1:k-1}) \\ & = \int p(y_k^{i-1,j-1}, y_k^{i,j-1}, y_k^{i-1,j}, y_k^{i,j}|e_k^{i,j}=1, \mathbf{x}_k) \\ & \qquad \times p(\mathbf{x}_k|e_k^{i,j}=1, \mathbf{y}_{1:k-1}) d\mathbf{x}_k. \end{aligned} \tag{26}$$

The first term in the integrand is (21) and the second term is the predicted pdf of an existing target's kinematic state in bin (i,j), whose expression will be calculated in Sec. IV-B. Now, applying the total probability theorem to the denominator in the first line of the RHS of (25)

$$\begin{aligned} & p(y_k^{i-1,j-1}, y_k^{i,j-1}, y_k^{i-1,j}, y_k^{i,j}|\mathbf{y}_{1:k-1}) = \\ & p(y_k^{i-1,j-1}, y_k^{i,j-1}, y_k^{i-1,j}, y_k^{i,j}|e_k^{i,j}=1, \mathbf{y}_{1:k-1}) P(e_k^{i,j}=1|\mathbf{y}_{1:k-1}) + \\ & p(y_k^{i-1,j-1}, y_k^{i,j-1}, y_k^{i-1,j}, y_k^{i,j}|e_k^{i,j}=0, \mathbf{y}_{1:k-1}) P(e_k^{i,j}=0|\mathbf{y}_{1:k-1}), \end{aligned} \tag{27}$$

which is obtained by combining (26) with (23) and (24).

B. pdf of an existing target's kinematic state

Under assumptions (4.1) and (4.2), the predicted target kinematic state pdf in bin (i,j) can be expanded over the presence of targets in bins $(m,n) \in N(i,j)$ at the previous time instant and the birth of a target in bin (i,j) at the current time instant

$$\begin{aligned} & p(\mathbf{x}_k|e_k^{i,j}=1, \mathbf{y}_{1:k-1}) = \\ & \frac{P_b^{i,j} P(e_{k-1}^{i,j}=0|\mathbf{y}_{1:k-1})}{P(e_k^{i,j}=1|\mathbf{y}_{1:k-1})} p(\mathbf{x}_k|e_k^{i,j}=1, e_{k-1}^{i,j}=0) \\ & + \sum_{(m,n)\in\mathcal{N}(i,j)} \frac{P(i,j|m,n,\mathbf{y}_{1:k-1})(1-P_d^{m,n}) P(e_{k-1}^{m,n}=1|\mathbf{y}_{1:k-1})}{P(e_k^{i,j}=1|\mathbf{y}_{1:k-1})} \\ & \qquad \times p(\mathbf{x}_k|e_k^{i,j}=1, e_{k-1}^{m,n}=1, \mathbf{y}_{1:k-1}). \end{aligned} \tag{28}$$

The proof is postponed to Appendix C.

Thus the predicted target kinematic state pdf in bin (i,j) can be interpreted as the weighted sum of several terms:

- the birth density $p(\mathbf{x}_k|e_k^{i,j}=1, e_{k-1}^{i,j}=0)$, defined previously as (16)

- the continuing density $p(\mathbf{x}_k|e_k^{i,j}=1, e_{k-1}^{i,j}=1, \mathbf{y}_{1:k-1})$, corresponding to a target that already existed in bin (i,j) at instant $k-1$
- the migration densities $p(\mathbf{x}_k|e_k^{i,j}=1, e_{k-1}^{m,n}=1, \mathbf{y}_{1:k-1})$, corresponding to targets existing in adjacent bins $(m,n) \in N(i,j) \setminus (i,j)$ at instant $k-1$ and migrating to bin (i,j) at instant k.

The continuing density is evaluated by marginalizing out the kinematic state at the previous time instant

$$\begin{aligned} &p(\mathbf{x}_k|e_k^{i,j}=1, e_{k-1}^{i,j}=1, \mathbf{y}_{1:k-1}) \\ &= \int p(\mathbf{x}_k, \mathbf{x}_{k-1}|e_k^{i,j}=1, e_{k-1}^{i,j}=1, \mathbf{y}_{1:k-1}) d\mathbf{x}_{k-1} \\ &= \int p(\mathbf{x}_k|\mathbf{x}_{k-1}, e_k^{i,j}=1, e_{k-1}^{i,j}=1) \\ &\qquad \times p(\mathbf{x}_{k-1}|e_{k-1}^{i,j}=1, \mathbf{y}_{1:k-1}) d\mathbf{x}_{k-1}, \end{aligned} \tag{29}$$

where in the third line, $p(\mathbf{x}_k|\mathbf{x}_{k-1}, e_k^{i,j}=1, e_{k-1}^{i,j}=1)$ is the intra-bin kinematic state transition pdf of Sec. III-B and $p(\mathbf{x}_{k-1}|e_{k-1}^{i,j}=1, \mathbf{y}_{1:k-1})$ is the target kinematic state pdf in bin (i,j) at the previous time instant. Similar expressions are obtained for the migration densities when $(m,n) \in N(i,j) \setminus (i,j)$

$$\begin{aligned} &p(\mathbf{x}_k|e_k^{i,j}=1, e_{k-1}^{m,n}=1, \mathbf{y}_{1:k-1}) = \\ &\int p(\mathbf{x}_k|\mathbf{x}_{k-1}, e_k^{i,j}=1, e_{k-1}^{m,n}=1) p(\mathbf{x}_{k-1}|e_{k-1}^{m,n}=1, \mathbf{y}_{1:k-1}) d\mathbf{x}_{k-1}, \end{aligned} \tag{30}$$

where $p(\mathbf{x}_k|\mathbf{x}_{k-1}, e_k^{i,j}=1, e_{k-1}^{m,n}=1)$ is the inter-bin kinematic state transition pdf of Sec. III-C and $p(\mathbf{x}_{k-1}|e_{k-1}^{m,n}=1, \mathbf{y}_{1:k-1})$ is the target kinematic state pdf in bin (m,n) at the previous time instant.

From Bayes's rule, we have

$$\begin{aligned} p(\mathbf{x}_k|e_k^{i,j}=1, \mathbf{y}_{1:k}) = &\frac{p(\mathbf{y}_k|e_k^{i,j}=1, \mathbf{x}_k, \mathbf{y}_{1:k-1})}{p(\mathbf{y}_k|e_k^{i,j}=1, \mathbf{y}_{1:k-1})} \\ &\times p(\mathbf{x}_k|e_k^{i,j}=1, \mathbf{y}_{1:k-1}). \end{aligned}$$

Now, applying the same approximation as in Appendix B (see Appendix D), a tractable Bayesian correction formula for the kinematic state pdf in bin (i,j) follows

$$\begin{aligned} &p(\mathbf{x}_k|e_k^{i,j}=1, \mathbf{y}_{1:k}) \\ &\quad \approx \frac{p(y_k^{i-1,j-1}, y_k^{i,j-1}, y_k^{i-1,j}, y_k^{i,j}|e_k^{i,j}=1, \mathbf{x}_k)}{p(y_k^{i-1,j-1}, y_k^{i,j-1}, y_k^{i-1,j}, y_k^{i,j}|e_k^{i,j}=1, \mathbf{y}_{1:k-1})} \\ &\quad \times p(\mathbf{x}_k|e_k^{i,j}=1, \mathbf{y}_{1:k-1}). \end{aligned} \tag{31}$$

The second line of (31) is a measurement likelihood ratio, whose numerator is given by (21) and whose denominator has been calculated as (26). The third line of (31) is the predicted kinematic state pdf in bin (i,j) given by (28).

Conditional on a target existence in bin (i,j), we define $\hat{\mathbf{x}}_{k|k}^{i,j} = [\hat{a}_{k|k}^{I\ i,j}, \hat{a}_{k|k}^{Q\ i,j}, \hat{b}_{k|k}^{I\ i,j}, \hat{b}_{k|k}^{Q\ i,j}, \hat{\tau}_{k|k}^{i,j}, \hat{\nu}_{k|k}^{i,j}, \hat{\zeta}_{k|k}^{i,j}]^T$ as the minimum mean-square error (MMSE) estimate of the kinematic state, containing the *a posteriori* estimate of the amplitudes, the delay, the Doppler and the Doppler rate. The expression of $\hat{\mathbf{x}}_{k|k}^{i,j}$ is given by

$$\hat{\mathbf{x}}_{k|k}^{i,j} = \int \mathbf{x}_k p(\mathbf{x}_k|e_k^{i,j}=1, \mathbf{y}_{1:k}) d\mathbf{x}_k. \tag{32}$$

C. Target detection and state estimation

In convential multitarget detection algorithms, the detection stage takes place before Bayesian filtering. TBD algorithms, on the contrary, perform detection and kinematic state estimation at the output of a Bayesian filter fed with raw measurements, to avoid information loss. A maximum posterior mode (MPM) approach for target detection is applied in each bin, followed by a MMSE criterion for kinematic state extraction, as described in Table I. The output of the algorithm is a list of bins containing detected targets, D_k, and the corresponding list of kinematic state estimates, E_k. Note that inconsistent bins, where the *a posteriori* delay estimate $\hat{\tau}_{k|k}^{i,j}$ (resp. Doppler estimate $\hat{\nu}_{k|k}^{i,j}$) falls outside the prescribed boundaries of the bin within a margin of $\pm t_{marg}$ (resp. $\pm f_{marg}$), are discarded.

$D_k = \emptyset$
$E_k = \emptyset$
for $i = 1$ to I **do**
  for $j = 1$ to J **do**
    Compute $P(e_k^{i,j} = 1|\mathbf{y}_{1:k})$ according to (25)
    Compute
    $\hat{\mathbf{x}}_{k|k}^{i,j} = [\hat{a}_{k|k}^{I\ i,j}, \hat{a}_{k|k}^{Q\ i,j}, \hat{b}_{k|k}^{I\ i,j}, \hat{b}_{k|k}^{Q\ i,j}, \hat{\tau}_{k|k}^{i,j}, \hat{\nu}_{k|k}^{i,j}, \hat{\zeta}_{k|k}^{i,j}]^T$
    according to (32)
    if $\hat{\tau}_{k|k}^{i,j} \notin [t_{i-1} - t_{marg}, t_i + t_{marg}]$ or
      $\hat{\nu}_{k|k}^{i,j} \notin [f_{j-1} - f_{marg}, f_j + f_{marg}]$ **then**
      $P(e_k^{i,j} = 1|\mathbf{y}_{1:k}) := 0$
      $p(\mathbf{x}_k|e_k^{i,j} = 1, \mathbf{y}_{1:k}) := \mathcal{N}\left(\mathbf{x}_k : \mathbf{x}_b^{i,j}, \mathbf{P}_b^{i,j}\right)$
    end if
    if $P(e_k^{i,j} = 1|\mathbf{y}_{1:k}) > 0.5$ **then**
      $D_k := \{D_k, (i,j)\}$
      $E_k := \{E_k, \hat{\mathbf{x}}_{k|k}^{i,j}\}$
    end if
  end for
end for

TABLE I
TARGET DETECTION AND KINEMATIC STATE ESTIMATION PROCEDURE AT INSTANT k.

D. Track classification

There are several issues associated with the simple detection scheme proposed in Sec. IV-C, which need to be treated. These issues can be related to the observation model, given by (21) and (23).

Firstly, this model is valid only if the apodized GAF (11) is negligible outside the extent of the delay/frequency bin where the hypothesized target is located. This assumption is valid for the low SNR targets of interest in TBD, but is violated for high SNR targets, especially when the delay and Doppler oversampling factors R_t and R_f are greater than one. Thus high SNR targets create redundant false tracks in neighboring bins, which must be detected and cancelled. This phenomenon is even amplified by the target existence probability prediction equation (24), which shows an inherent tendency for high SNR targets to "leak" into adjacent bins, especially when a target gets close to the boundaries of the bin in which it is located.

The second issue is the absence of superposition model for the observations in our work. Unlike the model retained in [20], there is no explicit way in (21) and (23) to model the fact that a given observation takes into account the contribution of several closely spaced targets. This implies that closely spaced targets cannot be allowed, so they must be merged, at least temporarily, to a single track.

A simple remedy to the issue of redundant and partially overlapping tracks which makes engineering sense, is to use guard bands [30]. Consider a given detected bin $(i,j) \in D_k$ containing a potential target (i.e. whose probability of target existence exceeds 50% according to the detection rule of Sec. IV-C), we assign the same class to all the detected bins located within $2R_t$ delay bins and $2R_f$ frequency bins. The resulting classification algorithm is explicited in Table II. Then, among all detected bins having the same class, the valid track is chosen as the one located in bin (i,j), which maximizes the *a posteriori* instantaneous energy defined as

$$E_{k|k}^{i,j} = \left(\hat{a}_{k|k}^{I\ i,j}\right)^2 + \left(\hat{a}_{k|k}^{Q\ i,j}\right)^2 + \left(\hat{b}_{k|k}^{I\ i,j}\right)^2 + \left(\hat{b}_{k|k}^{Q\ i,j}\right)^2.$$

Initialize a classification table $C = \mathbf{0}_{1\times|D_k|}$
class:=1
while at least one element of table C is equal to 0 **do**
  Let d_{first} be the index of the first element in table C such that $C[d_{first}] = 0$
  Retrieve the bin $(i,j) \leftarrow D_k[d_{first}]$ containing a target detection
  for $d = 1$ to $|D_k|$ **do**
    $(m,n) \leftarrow D_k[d]$
    if $|i-m| \leq 2R_t$ and $|j-n| \leq 2R_f$ **then**
      $C[d]$:=class
    end if
  end for
  class:=class+1
end while

TABLE II
CLASSIFICATION OF THE DETECTED BINS AT INSTANT k.

V. GAUSSIAN MIXTURE IMPLEMENTATION

In TBD systems, the observation model is in general nonlinear in the target state. In particular for the passive radar application of interest in the present paper, the observation model (21), conditional on a target existence in a given bin, is nonlinear. Therefore, the Bayesian recursion of Sec. IV requires some form of approximation, since the multiplication (31) in the correction step and the prediction integrals (29)-(30) cannot be expressed in closed form.

In the same spirit as the Gaussian sum filter [23], we approximate the target kinematic state pdf in each delay/frequency bin by a Gaussian mixture. Thus (32) is just the mean of the Gaussian mixture in the corresponding bin, which also greatly simplifies the target kinematic state extraction.

A. Prediction of the kinematic state

Assume that at instant $k-1$, the target kinematic state pdf in any delay/frequency bin (i,j) has the form

$$p(\mathbf{x}_{k-1}|e_{k-1}^{i,j}=1,\mathbf{y}_{1:k-1})=\mathcal{N}(\mathbf{x}_{k-1}:\mathbf{x}_{k-1|k-1}^{i,j},\mathbf{P}_{k-1|k-1}^{i,j}). \tag{33}$$

Then, for $(m,n)\in N(i,j)$, the expressions (29)-(30) have the form

$$\begin{aligned}&p(\mathbf{x}_k|e_k^{i,j}=1,e_{k-1}^{m,n}=1,\mathbf{y}_{1:k-1})\\&=\int p(\mathbf{x}_k|\mathbf{x}_{k-1},e_k^{i,j}=1,e_{k-1}^{m,n}=1)\\&\quad\times\mathcal{N}(\mathbf{x}_{k-1}:\mathbf{x}_{k-1|k-1}^{m,n},\mathbf{P}_{k-1|k-1}^{m,n})d\mathbf{x}_{k-1},\end{aligned}$$

where the kinematic state transition pdf $p(\mathbf{x}_k|\mathbf{x}_{k-1},e_k^{i,j}=1,e_{k-1}^{m,n}=1)$ is given by $\mathcal{N}\left(\mathbf{x}_k:f(\mathbf{x}_{k-1}),\mathbf{Q}\right)$ according to Sec. III-B and Sec. III-C (with a slight modification of $f(.)$ and $\mathbf{Q}$ indicated in Appendix A when $m=i$ and $n=j\pm1$). We recognize that the prediction integrals (29)-(30) correspond to the prediction step of the well-known extended Kalman filter [31], consequently

$\forall(m,n)\in N(i,j)$

$$p(\mathbf{x}_k|e_k^{i,j}=1,e_{k-1}^{m,n}=1,\mathbf{y}_{1:k-1})\approx\mathcal{N}(\mathbf{x}_k:\mathbf{x}_{k|k-1}^{m,n},\mathbf{P}_{k|k-1}^{m,n}), \tag{34}$$

where

$$\begin{cases}\mathbf{x}_{k|k-1}^{m,n}=f(\mathbf{x}_{k-1|k-1}^{m,n})\\ \mathbf{F}_k^{m,n}=\dfrac{\partial f(\mathbf{x}_{k-1})}{\partial\mathbf{x}_{k-1}}\Big|_{\mathbf{x}_{k-1}=\mathbf{x}_{k-1|k-1}^{m,n}}\\ \mathbf{P}_{k|k-1}^{m,n}=\mathbf{F}_k^{m,n}\mathbf{P}_{k-1|k-1}^{m,n}\mathbf{F}_k^{m,nT}+\mathbf{Q}\end{cases}$$

Injecting (16) and (34) into (28), we obtain a Gaussian mixture form for the prediction of the kinematic state pdf in bin (i,j)

$$\begin{aligned}&p(\mathbf{x}_k|e_k^{i,j}=1,\mathbf{y}_{1:k-1})\approx\\&\frac{P_b^{i,j}P(e_{k-1}^{i,j}=0|\mathbf{y}_{1:k-1})}{P(e_k^{i,j}=1|\mathbf{y}_{1:k-1})}\mathcal{N}\left(\mathbf{x}_k:\mathbf{x}_b^{i,j},\mathbf{P}_b^{i,j}\right)\\&+\sum_{(m,n)\in N(i,j)}\frac{P(i,j|m,n,\mathbf{y}_{1:k-1})(1-P_d^{m,n})P(e_{k-1}^{m,n}=1|\mathbf{y}_{1:k-1})}{P(e_k^{i,j}=1|\mathbf{y}_{1:k-1})}\\&\qquad\times\mathcal{N}(\mathbf{x}_k:\mathbf{x}_{k|k-1}^{m,n},\mathbf{P}_{k|k-1}^{m,n}).\end{aligned} \tag{35}$$

B. Correction of the kinematic state

Using (21) and (35), the numerator of the Bayesian correction equation (31) becomes

$$\begin{aligned}&p(y_k^{i-1,j-1},y_k^{i,j-1},y_k^{i-1,j},y_k^{i,j}|e_k^{i,j}=1,\mathbf{x}_k)p(\mathbf{x}_k|e_k^{i,j}=1,\mathbf{y}_{1:k-1})\approx\\&\frac{P_b^{i,j}P(e_{k-1}^{i,j}=0|\mathbf{y}_{1:k-1})}{P(e_k^{i,j}=1|\mathbf{y}_{1:k-1})}\mathcal{N}\left(\mathbf{x}_k:\mathbf{x}_b^{i,j},\mathbf{P}_b^{i,j}\right)\mathcal{N}\left(\mathbf{y}_k^{i,j}:h^{i,j}(\mathbf{x}_k),\mathbf{R}\right)\\&+\sum_{(m,n)\in N(i,j)}\frac{P(i,j|m,n,\mathbf{y}_{1:k-1})(1-P_d^{m,n})P(e_{k-1}^{m,n}=1|\mathbf{y}_{1:k-1})}{P(e_k^{i,j}=1|\mathbf{y}_{1:k-1})}\\&\qquad\times\mathcal{N}(\mathbf{x}_k:\mathbf{x}_{k|k-1}^{m,n},\mathbf{P}_{k|k-1}^{m,n})\mathcal{N}\left(\mathbf{y}_k^{i,j}:h^{i,j}(\mathbf{x}_k),\mathbf{R}\right).\end{aligned}$$

Regarding the products of Gaussians appearing in the previous formula, we easily recognize the correction step of the classical extended Kalman filter [31]. Therefore,

$$\begin{aligned}&\mathcal{N}\left(\mathbf{x}_k:\mathbf{x}_b^{i,j},\mathbf{P}_b^{i,j}\right)\mathcal{N}\left(\mathbf{y}_k^{i,j}:h^{i,j}(\mathbf{x}_k),\mathbf{R}\right)\\&\approx\mathcal{N}\left(\mathbf{y}_k^{i,j}:h^{i,j}(\mathbf{x}_b^{i,j}),\mathbf{H}_b^{i,j}\mathbf{P}_b^{i,j}\mathbf{H}_b^{i,jT}+\mathbf{R}\right)\\&\quad\times\mathcal{N}\left(\mathbf{x}_k:\mathbf{x}_{b|k}^{(i,j)},\mathbf{P}_{b|k}^{(i,j)}\right),\end{aligned}$$

where,

$$\begin{cases} \mathbf{H}_b^{i,j} = \dfrac{\partial h^{i,j}(\mathbf{x}_k)}{\partial \mathbf{x}_k}\Big|_{\mathbf{x}_k=\mathbf{x}_b^{i,j}} \\ \mathbf{K}_b^{i,j} = \mathbf{P}_b^{i,j}\mathbf{H}_b^{i,jT}\left(\mathbf{H}_b^{i,j}\mathbf{P}_b^{i,j}\mathbf{H}_b^{i,jT}+\mathbf{R}\right)^{-1} \\ \mathbf{x}_{b|k}^{(i,j)} = \mathbf{x}_b^{i,j} + \mathbf{K}_b^{i,j}\left(\mathbf{y}_k^{i,j} - h^{i,j}(\mathbf{x}_b^{i,j})\right) \\ \mathbf{P}_{b|k}^{(i,j)} = \mathbf{P}_b^{i,j} - \mathbf{K}_b^{i,j}\mathbf{H}_b^{i,j}\mathbf{P}_b^{i,j} \end{cases}$$

Using the same reasoning, we have

$$\begin{aligned} &\mathcal{N}(\mathbf{x}_k : \mathbf{x}_{k|k-1}^{m,n}, \mathbf{P}_{k|k-1}^{m,n})\mathcal{N}\left(\mathbf{y}_k^{i,j} : h^{i,j}(\mathbf{x}_k), \mathbf{R}\right) \\ \approx &\mathcal{N}\left(\mathbf{y}_k^{i,j} : h^{i,j}(\mathbf{x}_{k|k-1}^{m,n}), \mathbf{H}_k^{m,n}\mathbf{P}_{k|k-1}^{m,n}\mathbf{H}_k^{m,nT}+\mathbf{R}\right) \\ &\times \mathcal{N}\left(\mathbf{x}_k : \mathbf{x}_{k|k}^{(m,n)\to(i,j)}, \mathbf{P}_{k|k}^{(m,n)\to(i,j)}\right), \end{aligned}$$

where,

$$\begin{cases} \mathbf{H}_k^{m,n} = \dfrac{\partial h^{i,j}(\mathbf{x}_k)}{\partial \mathbf{x}_k}\Big|_{\mathbf{x}_k=\mathbf{x}_{k|k-1}^{m,n}} \\ \mathbf{K}_k^{m,n} = \mathbf{P}_{k|k-1}^{m,n}\mathbf{H}_k^{m,nT}\left(\mathbf{H}_k^{m,n}\mathbf{P}_{k|k-1}^{m,n}\mathbf{H}_k^{m,nT}+\mathbf{R}\right)^{-1} \\ \mathbf{x}_{k|k}^{(m,n)\to(i,j)} = \mathbf{x}_{k|k-1}^{m,n} + \mathbf{K}_k^{m,n}\left(\mathbf{y}_k^{i,j} - h^{i,j}(\mathbf{x}_{k|k-1}^{m,n})\right) \\ \mathbf{P}_{k|k}^{(m,n)\to(i,j)} = \mathbf{P}_{k|k-1}^{m,n} - \mathbf{K}_k^{m,n}\mathbf{H}_k^{m,n}\mathbf{P}_{k|k-1}^{m,n} \end{cases}$$

It follows that the numerator of the Bayesian correction step (31) for the kinematic state in bin (i,j) can be written as the Gaussian mixture

$$\begin{aligned} &p(y_k^{i-1,j-1}, y_k^{i,j-1}, y_k^{i-1,j}, y_k^{i,j}|e_k^{i,j}=1,\mathbf{x}_k)p(\mathbf{x}_k|e_k^{i,j}=1,\mathbf{y}_{1:k-1}) \approx \\ &\frac{P_b^{i,j}P(e_{k-1}^{i,j}=0|\mathbf{y}_{1:k-1})}{P(e_k^{i,j}=1|\mathbf{y}_{1:k-1})} \\ &\qquad\times \mathcal{N}\left(\mathbf{y}_k^{i,j} : h^{i,j}(\mathbf{x}_b^{i,j}), \mathbf{H}_b^{i,j}\mathbf{P}_b^{i,j}\mathbf{H}_b^{i,jT}+\mathbf{R}\right) \\ &\qquad\times \mathcal{N}\left(\mathbf{x}_k : \mathbf{x}_{b|k}^{(i,j)}, \mathbf{P}_{b|k}^{(i,j)}\right) \\ &+\sum_{(m,n)\in\mathcal{N}(i,j)} \frac{P(i,j|m,n,\mathbf{y}_{1:k-1})(1-P_d^{m,n})P(e_{k-1}^{m,n}=1|\mathbf{y}_{1:k-1})}{P(e_k^{i,j}=1|\mathbf{y}_{1:k-1})} \\ &\qquad\times \mathcal{N}\left(\mathbf{y}_k^{i,j} : h^{i,j}(\mathbf{x}_{k|k-1}^{m,n}), \mathbf{H}_k^{m,n}\mathbf{P}_{k|k-1}^{m,n}\mathbf{H}_k^{m,nT}+\mathbf{R}\right) \\ &\qquad\times \mathcal{N}\left(\mathbf{x}_k : \mathbf{x}_{k|k}^{(m,n)\to(i,j)}, \mathbf{P}_{k|k}^{(m,n)\to(i,j)}\right). \end{aligned} \tag{36}$$

Moreover, according to (26), the denominator of (31) is obtained by marginalizing out $\mathbf{x}_k$ in (36)

$$\begin{aligned} &p(y_k^{i-1,j-1}, y_k^{i,j-1}, y_k^{i-1,j}, y_k^{i,j}|e_k^{i,j}=1,\mathbf{y}_{1:k-1}) \approx \\ &\frac{P_b^{i,j}P(e_{k-1}^{i,j}=0|\mathbf{y}_{1:k-1})}{P(e_k^{i,j}=1|\mathbf{y}_{1:k-1})}\mathcal{N}\left(\mathbf{y}_k^{i,j} : h^{i,j}(\mathbf{x}_b^{i,j}), \mathbf{H}_b^{i,j}\mathbf{P}_b^{i,j}\mathbf{H}_b^{i,jT}+\mathbf{R}\right) \\ &+\sum_{(m,n)\in N(i,j)} \frac{P(i,j|m,n,\mathbf{y}_{1:k-1})(1-P_d^{m,n})P(e_{k-1}^{m,n}=1|\mathbf{y}_{1:k-1})}{P(e_k^{i,j}=1|\mathbf{y}_{1:k-1})} \\ &\qquad\times \mathcal{N}\left(\mathbf{y}_k^{i,j} : h^{i,j}(\mathbf{x}_{k|k-1}^{m,n}), \mathbf{H}_k^{m,n}\mathbf{P}_{k|k-1}^{m,n}\mathbf{H}_k^{m,nT}+\mathbf{R}\right). \end{aligned} \tag{37}$$

We also remind that (37) is sufficient to calculate the correction step of the target existence probability in bin (i,j) (see (25) and (27)).

Finally, to propagate the target kinematic state pdf at the next time instant, we need the Gaussian approximation (33) to hold also at instant k, otherwise the number of Gaussian components would grow with time. In other words, the Gaussian mixture approximation that we obtained for (31) must be collapsed to a single Gaussian of the form

$$p(\mathbf{x}_k|e_k^{i,j}=1,\mathbf{y}_{1:k}) = \mathcal{N}(\mathbf{x}_k : \mathbf{x}_{k|k}^{i,j}, \mathbf{P}_{k|k}^{i,j}). \tag{38}$$

using a moment-preserving merge [32]. This makes engineering sense, since it is desirable to keep the same computational complexity per bin at each time instant.

Remark 5.1: Note that $\mathbf{x}_{b|k}^{(i,j)}$ (resp. $\mathbf{P}_{b|k}^{(i,j)}$) represent the kinematic state estimate (resp. covariance matrix) corresponding to a target birth in bin (i,j) at instant k, given the present noisy observations. Similarly, $\mathbf{x}_{k|k}^{(m,n)\rightarrow(i,j)}$ (resp. $\mathbf{P}_{k|k}^{(m,n)\rightarrow(i,j)}$) represent the kinematic state estimate (resp. covariance matrix) corresponding to a target present in bin $(m,n) \in N(i,j)$ at instant $k-1$ and in bin (i,j) at instant k, given the past and present noisy observations. It appears that the computation of these quantities in each bin, originates from a bank of 6 parallel extended Kalman filters, one corresponding to a target birth, one corresponding to a target continuation in the same bin and 4 target migrations from adjacent bins. It is well known that the complexity of one recursion of the extended Kalman filter is $\mathcal{O}(N_x^3)$ [21], where N_x is the dimension of the target kinematic state. Therefore, the computational complexity of the Gaussian mixture implementation of the Bayesian multitarget detection and tracking algorithm of Sec. IV can be evaluated as $\mathcal{O}(6IJN_x^3)$ per iteration.

VI. Benchmark algorithms for multitarget detection / tracking

A. Batch processing TBD for multitarget detection and tracking

An interesting benchmark algorithm for our method is the batch processor proposed in [17]. Indeed, this TBD algorithm detects automatically the number of targets present in the environment and also jointly tracks their trajectories. This method relies on discretizing the state-space with a fixed grid. In our passive radar application, the state-space is the delay / frequency shift plane and the fixed grid is defined by (9). The total number of discrete states is therefore $(I+1)\times(J+1)$. Joint tracking and detection of multiple targets is achieved using a generalized likelihood ratio testing strategy (GLRT) [17], which reduces to a Viterbi tracking algorithm (VTA) [14], whose cost metric is the raw matched filter output associated with each discrete state. Due to the limitations in the target dynamics, we assume that each discrete state (i,j) can experience a state transition only towards one of the nine states centered on (i,j), from scan k to scan $k+1$. Coherent integration is performed over consecutive scans indexed by $k=1,\ldots,M$, where M is a parameter of choice equal to the depth of the VTA.

Assume that the maximum number of targets is fixed to K_{max}. In order to maintain a reasonable complexity without sacrificing the performances, K_{max} prospective targets are found using a suboptimum strategy, known as the single-pass successive-target-cancellation VTA (SP-STC-VTA) (we refer the reader to [17] for details). Basically, the method finds the K_{max} best admissible paths terminating at depth M using backtracking, with the constraint that two targets cannot be located at the same position at the same scan. In order to perform fair comparisons, we enforce the same constraint as in the classification algorithm of Table II: if there exists a scan $1 \leq k \leq M$, for which the current best tentative path is in state (m,n), while one of the previous best validated paths is in a state (i,j), such that $|i-m| \leq 2R_t$ and $|j-n| \leq 2R_f$, then the current best tentative path is discarded, otherwise it is validated.

The number of targets in the environment is estimated using the generalized Neyman-Pearson method proposed in [17]. The method depends on a Lagrange multiplier, whose value is chosen so as to achieve a fixed probability of false alarm. The selected tracks correspond to the best paths among the K_{max} validated paths at the output of the SP-STC-VTA.

Once a batch of M consecutive scans has been processed, the next batch is processed in exactly the same way. Fig. 4 illustrates the operations performed by the TBD batch processor.

Ignoring the contribution of backtracking and estimation of the number of targets, the computational complexity of the batch processor can be evaluated as $\mathcal{O}(9IJ)$ per scan.

Figure 4: About here.

B. JPDAF multitarget tracking

The JPDAF [11] is an interesting benchmark algorithm for our TBD method for several reasons. Firstly, the JPDAF is a well established classical method that uses thresholded matched filter outputs as observations. This will enable us to check the benefit of TBD on the passive radar application of interest in this paper. Secondly, JPDAF performs multitarget tracking, assuming that the correct number of targets is known. This will enable to check whether the proposed TBD algorithm, which has no prior knowledge on the time-varying number of targets, can detect automatically the birth and death of targets in the environment. Thirdly, the JPDAF is an assumed-density algorithm, very similar in spirit to the Gaussian mixture implementation of the proposed TBD algorithm. Based on all measurements that are likely to be assigned to a given target, the JPDAF computes the posterior distribution of the kinematic state as a Gaussian mixture, which is collapsed to a single Gaussian using moment-matching to ensure a constant complexity per iteration, exactly in the same way as in Sec. V.

Fig. 5 illustrates the complete detection and JPDAF multitarget tracking processing chain. After matched filtering and SVA apodization, at instant k, the set of raw measurements are thresholded to form the list D_k containing the (i,j) such that $|y_k^{i,j}| > \lambda$, where the threshold λ corresponds to the desired probability of false alarm, P_{fa}. It is well-known that each target is detected with probability P_d, which depends on P_{fa} and on the SNR. Since the derivation of the JPDAF enforces the constraint that each thresholded measurement can be assigned to at most one target [11], it is necessary to ensure that this constraint is verified for the application of interest. As mentioned previously in Sec. IV-D, this assumption is likely to be valid for the low SNR targets, but may be violated for high SNR targets, especially when the delay and Doppler oversampling factors R_t and R_f are greater than one. A simple workaround is to apply the classification algorithm of Table II to the list D_k, in order to avoid unwanted multiple measurements per target. Then, among all detected bins having the same class, the valid measurement is chosen as the one located in bin (i,j), which maximizes the instantaneous energy $|y_k^{i,j}|^2$. A set of thresholded measurements $\tilde{D}_k$ is formed by associating each retained bin (i,j) to the noisy delay/Doppler measurement $(t_0 + i\frac{1}{R_t B}, f_0 + j\frac{1}{R_f T})$. Using a

state-space representation similar to the one proposed in Sec. III-A, the new kinematic state vector $\tilde{\mathbf{x}}_k = [\tau_k, \nu_k, \zeta_k]^T$ follows the linear model

$$\begin{cases} \tilde{\mathbf{x}}_k = \mathbf{F}\tilde{\mathbf{x}}_{k-1} + \tilde{\mathbf{u}}_k \\ \tilde{\mathbf{y}}_k = \mathbf{H}\tilde{\mathbf{x}}_k + \tilde{\mathbf{n}}_k, \text{with} \quad \tilde{\mathbf{y}}_k \in \tilde{D}_k \end{cases} \tag{39}$$

where the process and measurement noises $\tilde{\mathbf{u}}_k$ and $\tilde{\mathbf{n}}_k$ are modeled as zero-mean independent, white Gaussian processes with covariance matrices $\tilde{\mathbf{Q}}$ and

$$\tilde{\mathbf{R}} = \text{diag}\{[(t_i - t_{i-1})^2/12, (f_i - f_{i-1})^2/12]\},$$

respectively. Moreover, the transition and measurement matrices are given by

$$\mathbf{F} = \begin{bmatrix} 1 & -\frac{T}{f_c} & 0 \\ 0 & 1 & T \\ 0 & 0 & 1 \end{bmatrix} \tag{40}$$

and

$$\mathbf{H} = \begin{bmatrix} 1 & 0 & 0 \\ 0 & 1 & 0 \end{bmatrix}. \tag{41}$$

Figure 5: About here.

By performing gating, the correct measurement for a given target, if detected, lies within the gate with probability close to one. This procedure makes the JPDAF efficient, since unlikely candidate measurements for association in $\tilde{D}_k$ are disregarded. Finally, the JPDAF [11] calculates the marginal posterior density of the kinematic state for each target as a Gaussian mixture, where each Gaussian component accounts for the fact that either one of the gated measurements in $\tilde{D}_k$ is correct or none of the gated measurements is correct. The mixture weights correspond to the association probabilities. Next, the Gaussian mixture is merged to a single Gaussian.

VII. Simulation results

A. Parameters

The position of the receive antenna in a 3D cartesian coordinate system is given by $\mathbf{x}_r = [0, 0, 0]^T$ and the position of the emitter is given by $\mathbf{x}_e = [-50 \times 10^3, -50 \times 10^3, -3]^T$, where all quantities are expressed in meters. The illuminator of opportunity sends a DAB signal using transmission mode I [5].

It follows that the duration of the useful part (resp. the guard interval) of an OFDM symbol is 1 ms (resp. 246 μs). So the duration of an OFDM symbol is 1246 μs. The number of transmitted subcarriers is 1536, therefore the total bandwidth is $B = 1.536$ MHz. Each subcarrier uses quadrature phase shift keying (QPSK) modulation. The carrier frequency is set to 230 MHz. We use a constant amplitude model (Swerling 0), which is reasonable considering that in the VHF frequency band, the target radar cross section (RCS) changes slowly with respect to the aspect angle [33].

Matched filtering is performed with an integration time T, corresponding to 32 consecutive OFDM symbols, which amounts to an integration gain of 47.87 dB. The matched filtering oversampling factor for the delay shift (resp. frequency shift) is chosen as $R_t = 1$ (resp. $R_f = 2$). This results in a delay bin of size $T_s = 1/R_t B \approx 0.65\mu$s and a frequency bin of size $1/R_f T \approx 12.54$ Hz. This validates the point target model adopted in this paper, since the bistatic range resolution is $c/B \approx 195$ m. The first delay shift $t_0 = 257/R_t B$ corresponds approximately to the propagation delay of the direct path between the emitter and the receiver and the extent of the surveillance volume is determined by the number of other delay shift samples, $I = 1150$. Due to the limitations imposed on target velocities, the frequency shifts of interest are in the interval $[-400, 400]$ Hz, so we set $f_0 = -400$ and $J = 64$.

For the proposed TBD method of Sec. IV, in the absence of prior information, we choose a uniform probability of target birth ($P_b^{i,j} = 10^{-5}$) and a uniform probability of target death ($P_d^{i,j} = 10^{-5}$) over all bins. Regarding the parameters of the intra-cell dynamics, the kinematic birth pdf is such that $\sigma_a = 100$, which corresponds approximately to a 40 dB SNR difference between the target with lowest and highest possible SNR, and σ_ζ is set to 5 Hz/s, so as to track targets with acceleration jumps up to several g's, where g denotes the acceleration of gravity. Similarly, in (14) which corresponds to the process equation of a continuing target, the autocorrelation matrix of the process noise is set to

$$\mathbf{Q} = \mathrm{diag}\{[0, 0, 0, 0, 0.01^2, 0.01^2, \sigma_\zeta^2]\}.$$

The parameters of the inter-cell dynamics were set by experimentation to $\alpha_\tau = 100 \times (R_t B)^2$ and $\alpha_\nu = 1$. Also, for the bin boundary margins of Sec. IV-C, $t_{marg} = 0$ and f_{marg} is equal to 5 percent of the size of a frequency bin.

The batch TBD method of Sec. VI-A uses the same matched filter and SVA apodization as the proposed TBD algorithm, followed by a SP-STC-VTA with depth $M = 5$ consecutive scans and backtracking over $K_{max} = 8$ prospective targets. The generalized Neyman-Pearson method for estimating the number of targets in the environment uses a Lagrange multiplier, whose value is chosen so as to achieve a fixed probability of false alarm equal to 10^{-4}.

The JPDAF method of Sec. VI-B also uses the same matched filter and SVA apodization as the proposed TBD algorithm, followed by a thresholding step such that the false alarm rate is fixed to $P_{fa} = 10^{-5}$. In order to test both methods in the same conditions, the autocorrelation matrix of the process noise in (39) is set to

$$\tilde{\mathbf{Q}} = \mathrm{diag}\{[0.01^2, 0.01^2, \sigma_\zeta^2]\}.$$

TABLE III
TARGET PARAMETERS FOR THE CONSTANT VELOCITY SCENARIO.

Target	SNR (dB) per sample	Initial position (km) $\mathbf{x}(t=0)$	Velocity (m/s) $\mathbf{v}(t)$	Birth instant (s)	Death instant (s)
Target 1	-34	$[70, 70, 10]^T$	$[200, 150, 0]^T$	0.4	1.6
Target 2	-14	$[-70, -70, 10]^T$	$[100, 100, 55]^T$	0.4	1.6
Target 3	-14	$[10, -60, 5]^T$	$[-100, -200, 20]^T$	0.4	1.4
Target 4	-34	$[50, -50, 0]^T$	$[-100, -40, 50]^T$	0.4	1.6
Target 5	-34	$[-50, -50, 2]^T$	$[70, 200, 60]^T$	0.4	1.6
Target 6	-34	$[30, 40, 20]^T$	$[180, -180, -50]^T$	0.4	1.4

TABLE IV
TARGET PARAMETERS FOR THE MANEUVERING SCENARIO.

Target	SNR (dB) per sample	Initial position (km) $\mathbf{x}(t=0)$	Initial Velocity (m/s) $\mathbf{v}(t=0)$	Peak acceleration
Target 1	-34	$[70, 70, 10]^T$	$[200, 150, 0]^T$	4 g
Target 2	-34	$[-70, -70, 10]^T$	$[100, 100, 55]^T$	4 g
Target 3	-34	$[10, -60, 5]^T$	$[-100, -200, 20]^T$	4 g

B. Constant velocity scenario with a time-varying number of targets

We first consider a scenario with a time-varying number of targets with constant velocity in the surveillance region. The parameters of the targets are given in Table III.

The proposed TBD method with Gaussian mixture implementation and the batch TBD method have no prior knowledge on the birth/death instants and kinematic state of the targets. On the contrary, the JPDAF method has perfect knowledge of the birth/death instants for each target. At the birth of each target, the JPDAF starts a new track with perfect kinematic state initialization. At the death of each target, the JPDAF drops the corresponding track. Targets with SNR per sample of -34 dB (resp. -14 dB) are detected with probability $P_d \approx 0.8$ (resp. $P_d \approx 1$) corresponding to $P_{fa} = 10^{-5}$. Thus, the prior information available to the JPDAF is equivalent to ideal target detection, so that the JPDAF merely performs multitarget tracking. For that reason, JPDAF serves as a benchmark to assess the performance of the TBD method, whose task is to perform multitarget detection and tracking jointly.

Fig. 6 (resp. Fig. 7) shows the true and estimated normalized bistatic delay (resp. Doppler shift) using the proposed TBD method for the scenario of Table III. We observe that the proposed algorithm detects all targets and that the birth and death instants are recovered satisfactorily. In general, the kinematic state is estimated with with good precision, except for a few time instants for the targets with lowest SNR. Indeed, we note that target 4 has one missed detection around $t = 0.86$ s and for target 6, the Doppler shift exhibits a small outlier around $t = 0.82$ s. A simple data association post-processing, similar to the association algorithms implemented in classical radar tracking (for example in the JPDAF), would easily solve the missed detection and outlier problem, though.

Fig. 8 (resp. Fig. 9) shows the true and estimated normalized bistatic delay (resp. Doppler shift) using the batch TBD method for the scenario of Table III. Thanks to the coherent integration over M consecutive scans, the batch TBD algorithm has good detection performances, since the number of targets along with the birth and death instants are recovered satisfactorily. However, the state estimates are either jagged around the correct trajectory (see for instance target 1 and 6 on Fig. 9) or experience a bias (see for instance target 2 and 3 on Fig. 9) . This phenomenon, visible on the Doppler estimates, is due to the fact that the SP-STC-VTA is forced to choose its sequence of state estimates among discrete values. Although not included due to lack of space, a zoom on the bistatic delay estimates would show exactly the same phenomenon.

Fig. 10 (resp. Fig. 11) shows the true and estimated normalized bistatic delay (resp. Doppler shift) using the JPDAF method for the scenario of Table III. The JPDAF has an inherent capacity to correct the missed detections and the outliers in addition to false alarm filtering, by performing data association. However, it is assumed that the time-varying number of targets is perfectly known. Another drawback of the JPDAF method comes from the discretization of the thresholded measurements into delay and frequency bins, which can introduce a relatively high bias and/or variance in the estimation of the kinematic state. This phenomenon is particularly apparent on the Doppler estimates of target 2 in Fig. 11.

Moreover, note that the SVA apodization step is very effective, otherwise the sidelobes of the two high SNR targets would have created false double tracks and also would have masked the weaker targets for all methods.

C. Maneuvering scenario

We also consider a maneuvering scenario with three targets subject to an acceleration jump. The characteristics of the targets are given in Table IV.

Fig. 12 (resp. Fig. 13) shows the true and estimated normalized bistatic delay (resp. Doppler shift) using the proposed TBD method for the maneuvering scenario of Table IV. The missed detection observed for target 1 around $t = 0.6$ s is not due to a loss of target track, as one may expect. This rather exemplifies an occasional behavior of the TBD algorithm, which can be explained as follows. When a target crosses the boundary of a frequency bin, occasionally the posterior target existence probability (25) temporarily drops below the 0.5 threshold imposed by the detection rule of Table I. A few (typically one ore two) time steps later, the posterior target existence probability will rise again above the threshold, thanks to the information gathered from future observations. A possible remedy for this occasional behavior could be to lower the detection threshold artificially for targets about to cross a frequency bin, or apply a simple data association post-processing to suppress the missed detections, as already advocated in Sec. VII-B. Nevertheless, a zoom on target 1 provided in Fig. 14 and Fig. 15, confirms that the detection of targets crossing several delay or frequency bins is in general not a problem, thanks to an appropriate choice of inter-bin dynamics in Sec. III-C. Also, the proposed TBD method is quite robust to severe acceleration jumps, despite the

fact that a simple near constant acceleration model was adopted to model the target dynamics.

Fig. 16 to 19 show the results for the maneuvering scenario of Table IV using the batch TBD method. In particular, the zoom on target 1, provided in Fig. 18 and Fig. 19 shows that the discrepency between the actual and estimated kinematic state can be quite large due to the discretization of the state-space into delay and frequency bins. Comparing Fig. 18 and 19 with Fig. 14 and 15, we notice that the batch TBD algorithm provides only a rough discretized estimate of the target trajectories, while the proposed TBD method provides significantly better tracking accuracy.

Fig. 20 to 23 show the results for the maneuvering scenario of Table IV using the JPDAF method. Again the data association performed by the JPDAF corrects the missed detections and the outliers and filters out the false alams. In particular, the zoom on target 1, provided in Fig. 22 and Fig. 23, reveals the effect of the discretization of the thresholded measurements into delay and frequency bins. The in-built Kalman filtering of the JPDAF is able to smooth out effectively the discretization effect on the delay shift estimates, as can be seen from Fig. 22. However, comparing Fig. 15 and Fig. 23, the proposed TBD method outperforms the JPDAF in terms of precision of the Doppler estimates. In particular, note that the proposed TBD algorithm recovers quasi instantaneously from the severe acceleration jump after $t = 1.2$ s, while the JPDAF will take time to do so.

These findings are confirmed by Monte Carlo simulations by simulating the maneuvering scenario of Table IV 100 times with independent observation noise realizations. The resulting performances in terms of RMSE are shown in Fig. 24 to 29. As expected, the RMSE of the bistatic delay for the batch TBD method oscillates between 0.03 (when the true continuous-valued state variable is equal to a discrete state) and 0.5 (when the true continuous-valued state variable is halfway between two discrete states) times the size of the bin used to discretize the state-space. Regarding the JPDAF method, after the beginning of the acceleration jump, the RMSE of the normalized delay shift experiences a severe overshoot for target 2 and 3, and then stabilizes to a value between 0.05 and 0.1. For the proposed TBD method, after the begin of the acceleration jump, the RMSE of the normalized delay shift experiences a moderate overshoot only for target 3, and then also stabilizes to a value between 0.05 and 0.1. However, the Doppler RMSE for the JPDAF is generally more than twice the value of the RMSE of the proposed method. Moreover, we observe that for target 1 in Fig. 29, the Doppler RMSE increases to a value almost equal to the frequency bin size, after the end of the acceleration jump. This behavior can be attributed to the bias in the JPDAF method mentioned before.

D. Comparison between the different approaches

The batch TBD processor is a fixed grid method able to detect targets accurately over the entire state-space. However, it provides only a rough estimate of the target's kinematic state as a byproduct, with unpredictable error spikes equal to half the size of the discretization bins, even for high SNR targets. Therefore, the batch TBD processor is suitable for applications,

where the detection of dim targets is of primary interest, while track accuracy is of secondary interest. Also, as for any batch algorithm, a processing latency equal to M scans must be tolerated before a new (resp. old) track can be detected (resp. deleted).

The JPDAF assumes prior knowledge of the number of targets and prior knowledge of the kinematic state when a track is initiated. Therefore, the JPDAF acts as a track maintenance algorithm. In practice, detection would have to be performed separately using an additional track initiation and deletion method [35]. The limitation of this two-step procedure is determined by the detection threshold. In order to detect the dim targets of interest in the present paper, the detection threshold must be set to a low value, which has two consequences. Firstly, this results in many false tracks being initiated from clutter measurements [35]. Secondly, the average number of scans needed to change the status (true or false) of a tentative track will increase [35]. Regarding the tracking performances, unlike the batch TBD algorithm, the JPDAF is a continuous-valued state estimation method, that delivers smoothed estimated target trajectories thanks to in-built Kalman filters. However, error spikes occur in the delay and Doppler estimates during abrupt changes of the target acceleration. Also, the JPDAF is a recursive method, which delivers new estimates at each scan without processing delay.

Thanks to its mixed discrete-continuous state-space representation, the proposed TBD method retains the best of both worlds, by performing Bayesian detection of a unknown number of multiple targets over the entire state-space on a per bin basis and joint tracking of the continuous-valued kinematic state within each bin. Also, the proposed TBD algorithm is recursive, thus without processing latency. Another benefit of the proposed TBD method is its ability to track targets with high acceleration jumps without the error spikes in the delay and Doppler estimates that one would expect to see for the simple near constant acceleration kinematic model advocated in the paper. Therefore, the passive radar application under consideration does not need multiple model approaches [34]. These benefits come at the cost of higher computational resources. On a 3.16 GHz Intel Xeon machine with a Matlab © implementation (without taking advantage of the high degree of parallelism that the methods offer), the average running time for processing 1.6 s of OFDM signal was equal to 190 min. for the proposed TBD method, 4.77 min. for the batch TBD method and 3.55 min. for the JPDAF method.

VIII. Conclusions

In the context of passive radars using illuminators of opportunity sending OFDM signals, the generalized ambiguity function (GAF) of the signal presents a high sidelobe level. For conventional radar techniques, based on thresholding the matched filter output, the sidelobes of high SNR targets would typically create false double tracks and mask low SNR targets. The proposed approach uses SVA apodization at the matched filter output sampled at a multiple of the Nyquist frequency, both in the delay and frequency shift domain, in order to cancel the sidelobes. As a result, the low SNR targets are revealed as well, but the

detection and tracking of such targets is known to be a difficult task. In this paper, we introduced a novel track-before-detect (TBD) method suitable for multitarget detection and tracking of an unknown and time-varying number of targets. We introduce a Bayesian framework based on a mixed discrete-continuous representation of the state-space in each delay/frequency bin induced by the matched filter sampling. The proposed algorithm performs detection by calculating the posterior probability of target existence, and tracking by computing the kinematic state probability density function conditional on a target existence, on a per bin basis. A suboptimal implementation based on a Gaussian mixture approximation is then introduced in order to get a tractable solution. Numerical experiments demonstrated the validity of the proposed approach for an illuminator of opportunity sending a DAB signal, in a non-maneuvering and a maneuvering multitarget scenario. Future developments will include the extension to passive multistatic and active monostatic radar systems.

Figure 6 to 29: About here.

APPENDIX A
KINEMATIC STATE TRANSITION PDF FOR A FREQUENCY BIN TRANSITION

For the frequency bin transition $(e_k^{i,j}=1, e_{k-1}^{i,j-1}=1)$, (12) is still valid, but (13) must be modified in the following manner

$$\begin{cases} a_k^I = \cos\left[2\pi(\nu_{k-1}-f_{j-1})T\right] b_{k-1}^I - \sin\left[2\pi(\nu_{k-1}-f_{j-1})T\right] b_{k-1}^Q \\ a_k^Q = \sin\left[2\pi(\nu_{k-1}-f_{j-1})T\right] b_{k-1}^I + \cos\left[2\pi(\nu_{k-1}-f_{j-1})T\right] b_{k-1}^Q \\ b_k^I \sim \mathcal{N}(b_k^I, 0, \sigma_a^2) \\ b_k^Q \sim \mathcal{N}(b_k^I, 0, \sigma_a^2) \\ \tau_k = \tau_{k-1} - \nu_{k-1}\frac{T}{f_c} \\ \nu_k = \nu_{k-1} + \zeta_{k-1}T \\ \zeta_k = \zeta_{k-1} \end{cases}$$

where the third and fourth equation take into account the sharp phase transition due to the frequency bin transition in a conservative manner, by applying to the state variables b_k^I and b_k^Q the same amplitude uncertainty as for a target birth, that is the amplitude dynamical range. We deduce the slight modification of $f(.)$ and $\mathbf{Q}$ required in (15) to obtain $p(\mathbf{x}_k|\mathbf{x}_{k-1}, e_k^{i,j}=1, e_{k-1}^{i,j-1}=1)$.

Similarly, for the frequency bin transition $(e_k^{i,j}=1, e_{k-1}^{i,j+1}=1)$, (12) is still valid, but (13) must be modified in the following manner

$$\begin{cases} a_k^I \sim \mathcal{N}(a_k^I, 0, \sigma_a^2) \\ a_k^Q \sim \mathcal{N}(a_k^I, 0, \sigma_a^2) \\ b_k^I = \cos\left[2\pi(\nu_{k-1}-f_j)T\right] a_{k-1}^I - \sin\left[2\pi(\nu_{k-1}-f_j)T\right] a_{k-1}^Q \\ b_k^Q = \sin\left[2\pi(\nu_{k-1}-f_j)T\right] a_{k-1}^I + \cos\left[2\pi(\nu_{k-1}-f_j)T\right] a_{k-1}^Q \\ \tau_k = \tau_{k-1} - \nu_{k-1}\frac{T}{f_c} \\ \nu_k = \nu_{k-1} + \zeta_{k-1}T \\ \zeta_k = \zeta_{k-1} \end{cases}$$

where the first and second equation take into account the sharp phase transition due to the frequency bin transition in a conservative manner, by applying to the state variables a_k^I and a_k^Q the same amplitude uncertainty as for a target birth, that is the amplitude dynamical range. We deduce the slight modification of $f(.)$ and $\mathbf{Q}$ required in (15) to obtain $p(\mathbf{x}_k|\mathbf{x}_{k-1}, e_k^{i,j}=1, e_{k-1}^{i,j+1}=1)$.

APPENDIX B
BAYESIAN CORRECTION FOR THE TARGET EXISTENCE PROBABILITIES

Using Bayes's rule, we obtain

$$\begin{aligned}
&P(e_k^{i,j}=1|\mathbf{y}_{1:k}) \\
&= \frac{p(\mathbf{y}_k|e_k^{i,j}=1,\mathbf{y}_{1:k-1})}{p(\mathbf{y}_k|\mathbf{y}_{1:k-1})} P(e_k^{i,j}=1|\mathbf{y}_{1:k-1}) \\
&= \frac{p\left(y_k^{i-1,j-1}, y_k^{i,j-1}, y_k^{i-1,j}, y_k^{i,j}, \mathbf{y}_k^* | e_k^{i,j}=1, \mathbf{y}_{1:k-1}\right)}{p\left(y_k^{i-1,j-1}, y_k^{i,j-1}, y_k^{i-1,j}, y_k^{i,j}, \mathbf{y}_k^* | \mathbf{y}_{1:k-1}\right)} \\
&\quad \times P(e_k^{i,j}=1|\mathbf{y}_{1:k-1}) \\
&= \frac{p\left(y_k^{i-1,j-1}, y_k^{i,j-1}, y_k^{i-1,j}, y_k^{i,j} | e_k^{i,j}=1, \mathbf{y}_{1:k-1}, \mathbf{y}_k^*\right)}{p\left(y_k^{i-1,j-1}, y_k^{i,j-1}, y_k^{i-1,j}, y_k^{i,j} | \mathbf{y}_{1:k-1}, \mathbf{y}_k^*\right)} \\
&\quad \times \frac{p\left(\mathbf{y}_k^* | e_k^{i,j}=1, \mathbf{y}_{1:k-1}\right)}{p\left(\mathbf{y}_k^* | \mathbf{y}_{1:k-1}\right)} \\
&\quad \times P(e_k^{i,j}=1|\mathbf{y}_{1:k-1}),
\end{aligned} \tag{42}$$

where $\mathbf{y}_k^* = \mathbf{y}_k \setminus \{y_k^{i-1,j-1}, y_k^{i,j-1}, y_k^{i-1,j}, y_k^{i,j}\}$. This formula holds exactly, but is intractable, since it involves long range dependencies between the matched filter outputs for a given integration window. Thanks to the thumbtack ambiguity diagram imposed by the apodization of Sec. II-C, matched filter outputs corresponding to different bins can be considered as statistically independent. Therefore, we can neglect the dependence of $y_k^{i-1,j-1}, y_k^{i,j-1}, y_k^{i-1,j}, y_k^{i,j}$ on $\mathbf{y}_k^*$ (see also the discussion in Rem 2.4 and 2.5). For similar reasons, the following approximation holds

$$p(\mathbf{y}_k^*|e_k^{i,j}=1,\mathbf{y}_{1:k-1}) \approx p(\mathbf{y}_k^*|\mathbf{y}_{1:k-1})$$

(see the discussion in Sec. III-A).

Therefore, the desired result (25) follows.

APPENDIX C
PROOF OF THE TARGET KINEMATIC STATE PREDICTION FORMULA

Applying the total probability theorem, we have

$$\begin{aligned}
&p(\mathbf{x}_k|e_k^{i,j}=1,\mathbf{y}_{1:k-1}) = \\
&p(\mathbf{x}_k|e_k^{i,j}=1,e_{k-1}^{i,j}=0,\mathbf{y}_{1:k-1}) P(e_{k-1}^{i,j}=0|e_k^{i,j}=1,\mathbf{y}_{1:k-1}) \\
&+ \sum_{(m,n)\in N(i,j)} p(\mathbf{x}_k|e_k^{i,j}=1,e_{k-1}^{m,n}=1,\mathbf{y}_{1:k-1}) \\
&\qquad \times P(e_{k-1}^{m,n}=1|e_k^{i,j}=1,\mathbf{y}_{1:k-1}).
\end{aligned} \tag{43}$$

Note that $p(\mathbf{x}_k|e_k^{i,j}=1,e_{k-1}^{i,j}=0,\mathbf{y}_{1:k-1})$ is the kinematic state birth pdf in bin (i,j), therefore the dependence on $\mathbf{y}_{1:k-1}$ can be dropped.

Let us first calculate $P(e_{k-1}^{i,j}=0|e_k^{i,j}=1,\mathbf{y}_{1:k-1})$ using Bayes's rule

$$\begin{aligned}
&P(e_{k-1}^{i,j}=0|e_k^{i,j}=1,\mathbf{y}_{1:k-1}) \\
&= \frac{P(e_k^{i,j}=1|e_{k-1}^{i,j}=0,\mathbf{y}_{1:k-1}) P(e_{k-1}^{i,j}=0|\mathbf{y}_{1:k-1})}{P(e_k^{i,j}=1|\mathbf{y}_{1:k-1})}.
\end{aligned}$$

Since $P(e_k^{i,j}=1|e_{k-1}^{i,j}=0,\mathbf{y}_{1:k-1})$ represents the *a priori* probability of target birth in bin (i,j) at instant k, which is independent of the past observations, we obtain

$$P(e_{k-1}^{i,j}=0|e_k^{i,j}=1,\mathbf{y}_{1:k-1}) = \frac{P_b^{i,j} P(e_{k-1}^{i,j}=0|\mathbf{y}_{1:k-1})}{P(e_k^{i,j}=1|\mathbf{y}_{1:k-1})}. \tag{44}$$

In the same way, let us apply Bayes's rule to calculate $P(e_{k-1}^{m,n}=1|e_k^{i,j}=1,\mathbf{y}_{1:k-1})$ when $(m,n)\in N(i,j)$

$$\begin{aligned}&P(e_{k-1}^{m,n}=1|e_k^{i,j}=1,\mathbf{y}_{1:k-1})\\&=\frac{P(e_k^{i,j}=1|e_{k-1}^{m,n}=1,\mathbf{y}_{1:k-1})P(e_{k-1}^{m,n}=1|\mathbf{y}_{1:k-1})}{P(e_k^{i,j}=1|\mathbf{y}_{1:k-1})},\end{aligned}$$

where $P(e_k^{i,j}=1|e_{k-1}^{m,n}=1,\mathbf{y}_{1:k-1})$ represents the probability of target existence in bin (i,j) at instant k, given that a target exists at the previous instant in bin $(m,n)\in N(i,j)$ and given the set of past observations. Using the notations and assumptions introduced in Sec. III-C, we have

$$P(e_k^{i,j}=1|e_{k-1}^{m,n}=1,\mathbf{y}_{1:k-1})=P(i,j|m,n,\mathbf{y}_{1:k-1})(1-P_d^{m,n}).$$

Thus

$$\begin{aligned}&P(e_{k-1}^{m,n}=1|e_k^{i,j}=1,\mathbf{y}_{1:k-1})\\&=\frac{P(i,j|m,n,\mathbf{y}_{1:k-1})(1-P_d^{m,n})P(e_{k-1}^{m,n}=1|\mathbf{y}_{1:k-1})}{P(e_k^{i,j}=1|\mathbf{y}_{1:k-1})}.\end{aligned}\tag{45}$$

Injecting (44) and (45) into (43) completes the proof.

APPENDIX D
BAYESIAN CORRECTION FOR THE TARGET KINEMATIC STATE

Using Bayes's rule, we obtain

$$\begin{aligned}&\frac{p(\mathbf{y}_k|e_k^{i,j}=1,\mathbf{x}_k,\mathbf{y}_{1:k-1})}{p(\mathbf{y}_k|e_k^{i,j}=1,\mathbf{y}_{1:k-1})}\\&=\frac{p\left(y_k^{i-1,j-1},y_k^{i,j-1},y_k^{i-1,j},y_k^{i,j},\mathbf{y}_k^*|e_k^{i,j}=1,\mathbf{x}_k,\mathbf{y}_{1:k-1}\right)}{p\left(y_k^{i-1,j-1},y_k^{i,j-1},y_k^{i-1,j},y_k^{i,j},\mathbf{y}_k^*|e_k^{i,j}=1,\mathbf{y}_{1:k-1}\right)}\\&=\frac{p\left(y_k^{i-1,j-1},y_k^{i,j-1},y_k^{i-1,j},y_k^{i,j}|e_k^{i,j}=1,\mathbf{x}_k,\mathbf{y}_{1:k-1},\mathbf{y}_k^*\right)}{p\left(y_k^{i-1,j-1},y_k^{i,j-1},y_k^{i-1,j},y_k^{i,j}|e_k^{i,j}=1,\mathbf{y}_{1:k-1},\mathbf{y}_k^*\right)}\\&\quad\times\frac{p\left(\mathbf{y}_k^*|e_k^{i,j}=1,\mathbf{x}_k,\mathbf{y}_{1:k-1}\right)}{p\left(\mathbf{y}_k^*|e_k^{i,j}=1,\mathbf{y}_{1:k-1}\right)}\end{aligned}\tag{46}$$

Using the same arguments as in Appendix B, matched filter outputs corresponding to different bins can be considered as approximately statistically independent. Therefore, we can neglect the dependence of $y_k^{i-1,j-1},y_k^{i,j-1},y_k^{i-1,j},y_k^{i,j}$ on $\mathbf{y}_k^*$. Also, $\mathbf{y}_k^*$ depends neither on the presence of a target in bin (i,j) nor on its kinematic state, so

$$\begin{aligned}p(\mathbf{y}_k^*|e_k^{i,j}=1,\mathbf{x}_k,\mathbf{y}_{1:k-1})&\approx p(\mathbf{y}_k^*|\mathbf{y}_{1:k-1})\\p(\mathbf{y}_k^*|e_k^{i,j}=1,\mathbf{y}_{1:k-1})&\approx p(\mathbf{y}_k^*|\mathbf{y}_{1:k-1}).\end{aligned}$$

Therefore the following approximation is valid

$$\begin{aligned}&\frac{p(\mathbf{y}_k|e_k^{i,j}=1,\mathbf{x}_k,\mathbf{y}_{1:k-1})}{p(\mathbf{y}_k|e_k^{i,j}=1,\mathbf{y}_{1:k-1})}\\&\approx\frac{p\left(y_k^{i-1,j-1},y_k^{i,j-1},y_k^{i-1,j},y_k^{i,j}|e_k^{i,j}=1,\mathbf{x}_k,\mathbf{y}_{1:k-1}\right)}{p\left(y_k^{i-1,j-1},y_k^{i,j-1},y_k^{i-1,j},y_k^{i,j}|e_k^{i,j}=1,\mathbf{y}_{1:k-1}\right)}.\end{aligned}$$

Finally, considering (21), the matched filter outputs $y_k^{i-1,j-1},y_k^{i,j-1},y_k^{i-1,j},y_k^{i,j}$ conditioned on $\mathbf{x}_k$ given that $e_k^{i,j}=1$ are independent of $\mathbf{y}_{1:k-1}$. Therefore, the desired result (31) follows.

APPENDIX E
NOISE STATISTICS AT THE MATCHED FILTER OUTPUT

The noise contribution before matched filtering $w(t)$ is modeled as a zero-mean AWGN with variance σ^2. Thus

$$\begin{aligned} &E[w(\theta)] = 0 \\ &E[w(\theta_1)w(\theta_2)^*] = \sigma^2\delta(\theta_1 - \theta_2). \end{aligned} \tag{47}$$

Consider the noise contribution $z_k(t,f)$ at the matched filter output corresponding to a delay shift t and a frequency shift f, as given by (4). The expectation can be written as

$$E[z_k(t,f)] = \frac{1}{T}\int_{kT-T/2}^{(k+1)T-T/2} E[w(\theta)]s_{ref}(\theta - t)^* e^{-j2\pi f\theta}d\theta,$$

where $s_{ref}(t)$ is considered as a known deterministic signal, since we assume perfect recovery of the reference signal at the reference antenna. Therefore, according to (47), $E[z_k(t,f)] = 0$.

Moreover, we have

$$\begin{aligned} &E[z_k(t,f)z_k(t-\theta, f-\varphi)^*] = \\ &E\Big\{\frac{1}{T}\int_{kT-T/2}^{(k+1)T-T/2} w(\theta_1)s_{ref}(\theta_1 - t)^* e^{-j2\pi f\theta_1}d\theta_1 \\ &\quad\times\frac{1}{T}\int_{kT-T/2}^{(k+1)T-T/2} w(\theta_2)^* s_{ref}(\theta_2 - t + \theta)e^{j2\pi(f-\varphi)\theta_2}d\theta_2\Big\} \\ =&\frac{1}{T^2}E\Big\{\int_{kT-T/2}^{(k+1)T-T/2}\int_{kT-T/2}^{(k+1)T-T/2} w(\theta_1)w(\theta_2)^* s_{ref}(\theta_1 - t)^* \\ &\qquad\times s_{ref}(\theta_2 - t + \theta)e^{-j2\pi f\theta_1}e^{j2\pi(f-\varphi)\theta_2}d\theta_1 d\theta_2\Big\} \end{aligned}$$

Exchanging the order of the expectation and the double integration, we obtain

$$\begin{aligned} &E[z_k(t,f)z_k(t-\theta, f-\varphi)^*] \\ =&\frac{1}{T^2}\int_{kT-T/2}^{(k+1)T-T/2}\int_{kT-T/2}^{(k+1)T-T/2} E[w(\theta_1)w(\theta_2)^*] \\ &\quad\times s_{ref}(\theta_1 - t)^* s_{ref}(\theta_2 - t + \theta)e^{-j2\pi f\theta_1}e^{j2\pi(f-\varphi)\theta_2}d\theta_1 d\theta_2 \end{aligned}$$

Now, using (47), the double integral reduces to the following single integral

$$\begin{aligned} &E[z_k(t,f)z_k(t-\theta, f-\varphi)^*] \\ =&\frac{\sigma^2}{T^2}\int_{kT-T/2}^{(k+1)T-T/2} s_{ref}(\theta_1 - t)^* s_{ref}(\theta_1 - t + \theta) \\ &\qquad\times e^{-j2\pi f\theta_1}e^{j2\pi(f-\varphi)\theta_1}d\theta_1 \\ =&\frac{\sigma^2}{T^2}\int_{kT-T/2}^{(k+1)T-T/2} s_{ref}(\theta_1 - t)^* s_{ref}(\theta_1 - t + \theta)e^{-j2\pi\varphi\theta_1}d\theta_1 \end{aligned}$$

Applying the change of variable $u = \theta_1 - t - kT$, we obtain

$$\begin{aligned}
&E[z_k(t,f)z_k(t-\theta,f-\varphi)^*] \\
=&\frac{\sigma^2}{T^2}\int_{-T/2-t}^{T/2-t} s_{ref}(u+kT+\theta)s_{ref}(u+kT)^* e^{-j2\pi\varphi(u+t+kT)}du \\
=&\frac{\sigma^2}{T}e^{-j2\pi\varphi(t+kT)} \\
&\times\frac{1}{T}\int_{-T/2-t}^{T/2-t} s_{ref}(u+kT+\theta)s_{ref}(u+kT)^* e^{-j2\pi\varphi u}du \\
=&\frac{\sigma^2}{T}e^{-j2\pi\varphi(t+kT)} \\
&\times\frac{1}{T}\int_{-T/2-t}^{T/2-t} s(u+kT+\theta)s_{ref}(u+kT)^* e^{-j2\pi\varphi u}du,
\end{aligned}$$

where the last equation holds because, as mentioned in Sec. II-B, the reference signal $s_{ref}(t)$ is nothing but the transmitted signal $s(t)$ with guard interval and pilot carriers modification advocated in [9] to remove the side-peaks.

Finally, considering that for OFDM signals $t \ll T$ and that the GAF defined by (6) is invariant to a timing advance of kT, we obtain

$$E[z_k(t,f)z_k(t-\theta,f-\varphi)^*] = \frac{\sigma^2}{T}\chi(\theta,\varphi)e^{-j2\pi\varphi(t+kT)}.$$

REFERENCES

[1] Willis, N.J.
Bistatic Radar.
Artech House, 1991.

[2] Sahr, J.D. and Lind, F.D.
The Manastash Ridge radar: a passive bistatic radar for upper atmospheric radio science.
Radio Science, **32**, 6 (1997), 2345-2358.

[3] Baker, C.J. and Griffiths, H.D.
Bistatic and multistatic radar sensors for homeland security.
In *Advances in sensing with security applications*, NATO Security through Science Series, vol. 2, 2006.

[4] Griffiths, H.D. and Baker, C.J.
Measurement and analysis of ambiguity functions of passive radar transmissions.
In *Proc. of the IEEE International Radar Conference*, 2005, 321-325.

[5] ETS 300 401.
Radio broadcasting systems; Digital audio broadcasting (DAB) to mobile, portable and fixed receivers.
European Telecommunications Standard Institute, 2001.

[6] ETS 300 744.
Digital video broadcasting (DVB); framing structure, channel coding and modulation for digital terrestrial television (DVB-T).
European Telecommunications Standard Institute, 1997.

[7] Poulin, D.
Passive detection using digital broadcasters (DAB, DVB) with COFDM modulation.
IEE Proc. Radar Sonar and Navigation, **152**, 3 (2005), 143-152.

[8] Coleman, C. and Yardley, H.
Passive bistatic radar based on target illuminations by digital audio broadcasting.
IET Radar Sonar and Navigation, **2**, 5 (2008), 366-375.

[9] Saini, R. and Cherniakov, M.
DTV signal ambiguity function analysis for radar application.
IEE Proc. Radar Sonar and Navigation, **152**, 3 (2005), 133-142.

[10] Reid, D.
An algorithm for tracking multiple targets.
IEEE Trans. on Automatic Control, **24**, 6 (1979), 843-854.

[11] Fortmann, T., Bar-Shalom, Y. and Scheffe, M.
Sonar tracking of multiple targets using joint probabilistic data association.
IEEE Journal of Oceanic Engineering, **8**, 3 (1983), 173-184.

[12] Mahler, R.
Multitarget Bayes filtering via first-order multitarget moments.
IEEE Trans. on Aerospace and Electronic Systems, **39**, 4 (2003), 1152-1178.

[13] Barniv, Y.
Dynamic programming solution for detecting dim moving targets.
IEEE Trans. on Aerospace and Electronic Systems, **21**, 1 (1985), 144-156.

[14] Buzzi S., Lops M. and Venturino L.
Track-before-detect procedures for early detection of moving target from airborne radars.

IEEE Trans. on Aerospace and Electronic Systems, **41**, 1 (2005), 937-954.
[15] Orlando D., Venturino L., Lops M. and Ricci G.
Track-before-detect strategies for STAP radars.
IEEE Trans. on Signal Procesing, **58**, 1 (2010), 933-938.
[16] Orlando D., Ehlers F. and Ricci G.
Track-before-detect algorithms for bistatic sonars.
In *Proc. of the the 2nd International Workshop on Cognitive Information Processing*, 2010, 3755-3760.
[17] Buzzi S., Lops M., Venturino L. and Ferri M.
Track-before-detect procedures in a multi-target environment.
IEEE Trans. on Aerospace and Electronic Systems, **44**, 1 (2008), 1135-1150.
[18] Salmond D.J. and Birch, H.
A particle filter for track-before-detect.
In *Proc. of the American Control Conference*, 2001, 3755-3760.
[19] Rutten, M.G., Gordon, N.J. and Maskell, S.
Recursive track-before-detect with target amplitude fluctuations.
IEE Proc. Radar Sonar and Navigation, **152**, 5 (2005), 345-352.
[20] Boers, Y. and Driessen, J.N.
Multitarget particle filter track before detect application.
IEE Proc. Radar Sonar and Navigation, **151**, 5 (2004), 351-357.
[21] Daum, F.
Nonlinear filters: beyond the Kalman filter.
IEEE A&E Systems Magazine, **20**, 8 (2005), 57-69.
[22] Skolnik, M.I.
Introduction to radar systems.
McGraw-Hill, 2001.
[23] Sorensen, H.W. and Alspach, D.L.
Recursive bayesian filtering using Gaussian sums.
Automatica, **7**, (1971) 465-479.
[24] Berger, C. R., Demissie, B., Heckenbach, J., Willett, P. and Zhou, S.
Signal processing for passive radar using OFDM waveforms.
IEEE J. of Selected Topics in Signal Processing, **4**, 1 (2010), 226-238.
[25] van Waterschoot, T., Le Nir, V., Duplicy, J., Moonen, M.
Analytical expressions for the power spectral density of CP-OFDM and ZP-OFDM signals.
IEEE Signal Processing Letters, **17**, 4 (2010), 371-374.
[26] Stankwitz, H.C., Dallaire, R.J. and Fienup, J.R.
Nonlinear apodization for sidelobe control in SAR imagery.
IEEE Trans. on Aerospace and Electronic Systems, **31**, 1 (1995), 267-279.
[27] Lee, J.A.C. and Munson, D.C.
Spatially variant apodization for image reconstruction from partial Fourier data.
IEEE Trans. on Image Processing, **9**, 11 (2000), 1914-1925.
[28] Pastina, D., Colone, F. and Lombardo, P.
Effect of apodization on SAR image understanding.
IEEE Trans. on Geoscience and Remote Sensing, **45**, 11 (2007), 3533-3551.
[29] Shi, Q.
ICI mitigation for OFDM using PEKF.
IEEE Signal Processing Letters, **17**, 12 (2010), 981-984.
[30] Bethel, R.E. and Paras, G.J.
A PDF multitarget tracker.
IEEE Trans. on Aerospace and Electronic Systems, **30**, 2 (1994), 386-403.
[31] Anderson, B.D.O. and Moore, J.B.
Optimal filtering.
Englewood Cliffs, N.J.: Prentice Hall, 1979.
[32] Runnalls, A.R.
Kullback-Leibler approach to Gaussian mixture reduction.
IEEE Trans. on Aerospace and Electronic Systems, **43**, 3 (2007), 989-999.
[33] Balajti, I.
RCS aspects of multiband radar systems composed of “VHF”, “L” and “X” band radars.
In *Proc. of the International Conference on Microwaves, Radar and Wireless Communications*, 2006, 1149-1155.
[34] Mazor, E., Averbuch, A., Bar-Shalom, Y. and Dayan, J.
Interacting multiple model methods in target tracking: a survey.
IEEE Trans. on Aerospace and Electronic Systems, **34**, 1 (1998), 103-123.
[35] Blackman, S. and Popoli, R.
Design and analysis of modern tracking systems.
Artech House, 1999.

Frederic Lehmann received the E.E. degree and the M.S.E.E. degree from ENSERG, France, in 1998. In 2002, he received the PhD in Electrical Engineering from the National Polytechnical Institute, Grenoble (INPG), France. He worked as a Research Engineer with STMicroelectronics from 1999 to 2002. From 2003 to 2004 he was a Post-doctoral Researcher at LAAS (Laboratory for Analysis and Architecture of Systems), CNRS, Toulouse, France. Currently, he is an Assistant Professor at Institut TELECOM, Telecom SudParis, Evry, France. His main research interests are in the area of communication theory and non-linear signal processing applied to radar and wireless transmissions.

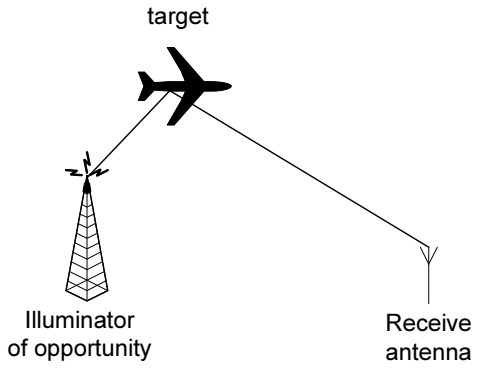

Fig. 1. Passive radar system with stationary emitter and receiver.

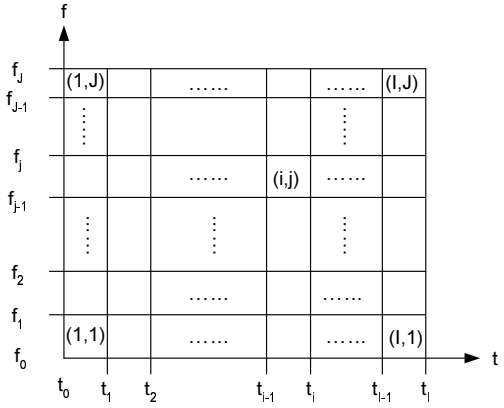

Fig. 2. Delay/frequency plane partitioned into bins of equal size.

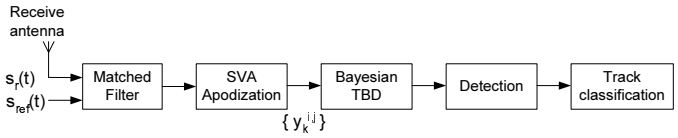

Fig. 3. Proposed TBD multitarget detection and tracking processing chain.

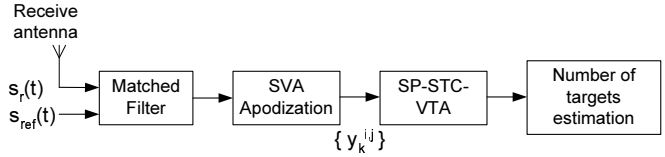

Fig. 4. Batch TBD multitarget detection and tracking processing chain.

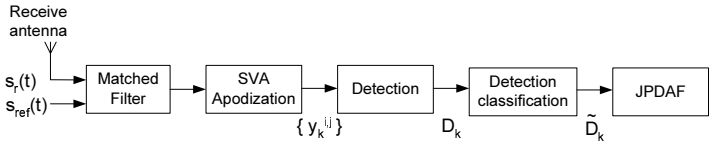

Fig. 5. Detection and JPDAF multitarget tracking processing chain.

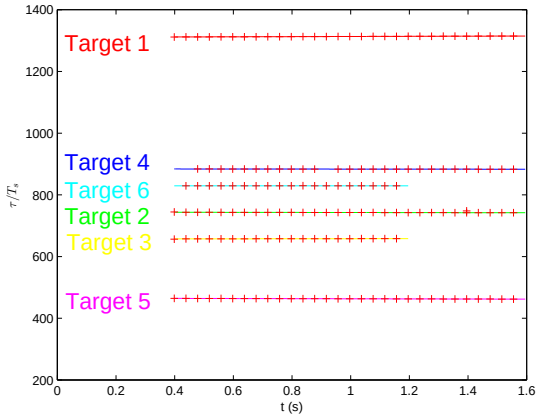

Fig. 6. Normalized bistatic delay in the constant velocity scenario: true position (solid) and proposed TBD estimates (+).

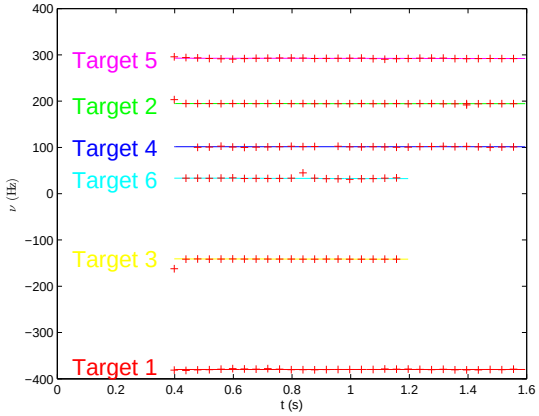

Fig. 7. Doppler shift in the constant velocity scenario: true position (solid) and proposed TBD estimates (+).

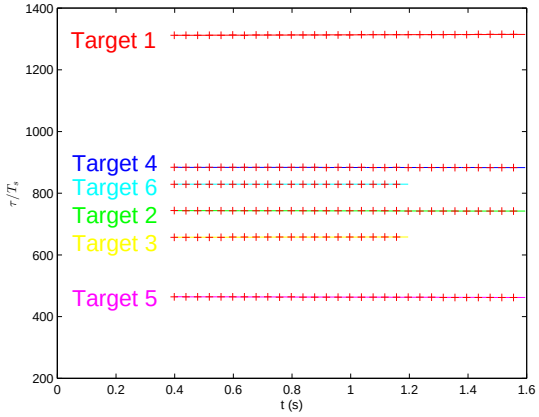

Fig. 8. Normalized bistatic delay in the constant velocity scenario: true position (solid) and batch TBD estimates (+).

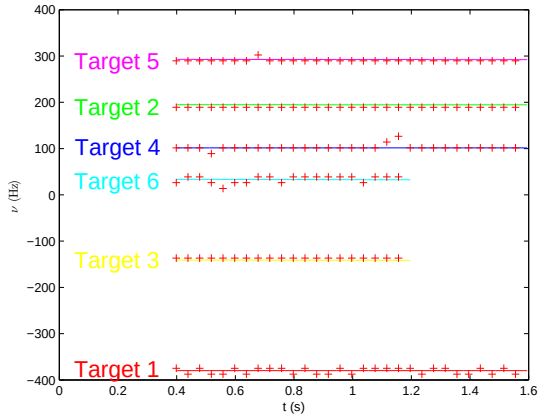

Fig. 9. Doppler shift in the constant velocity scenario: true position (solid) and batch TBD estimates (+).

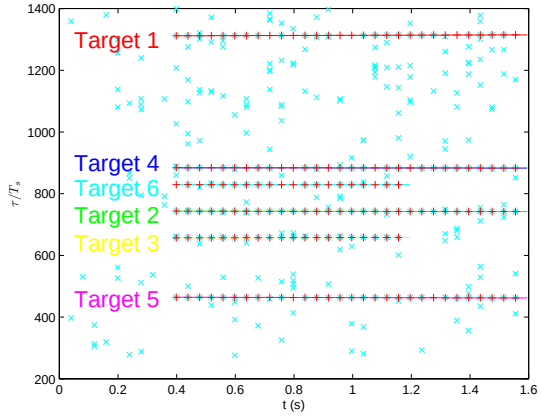

Fig. 10. Normalized bistatic delay in the constant velocity scenario: true position (solid), thresholded measurements (x) and JPDAF estimates (+).

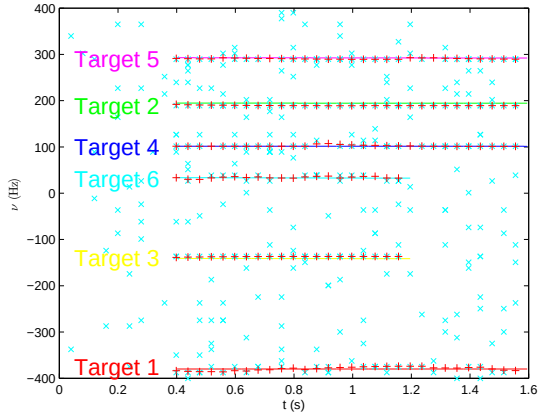

Fig. 11. Doppler shift in the constant velocity scenario: true position (solid), thresholded measurements (x) and JPDAF estimates (+).

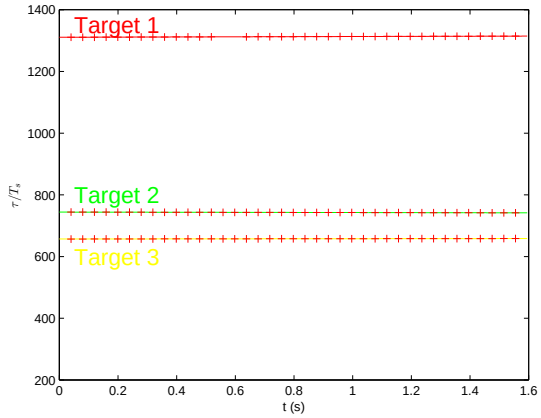

Fig. 12. Normalized bistatic delay in the maneuvering scenario: true position (solid) and proposed TBD estimates (+).

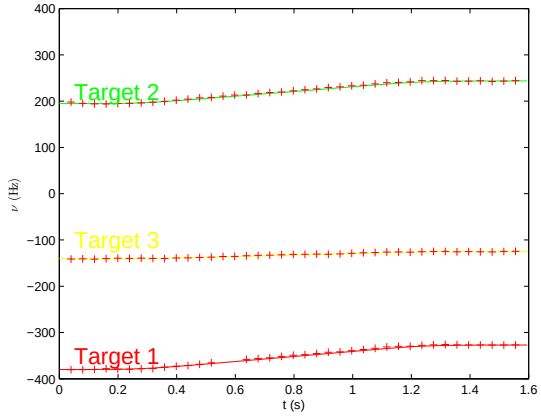

Fig. 13. Doppler shift in the maneuvering scenario: true position (solid) and proposed TBD estimates (+).

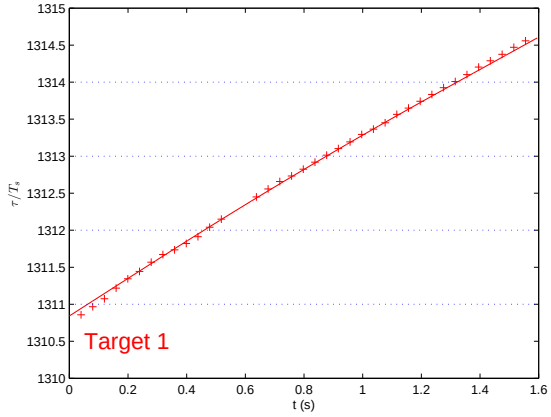

Fig. 14. Normalized bistatic delay in the maneuvering scenario for target 1: true position (solid) and proposed TBD estimates (+). The horizontal dotted lines represent the boundaries of the delay bins.

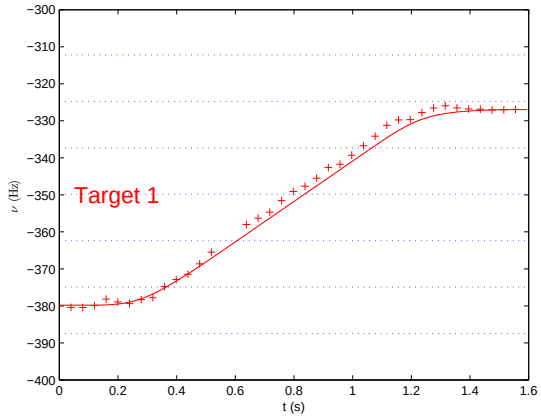

Fig. 15. Doppler shift in the maneuvering scenario for target 1: true position (solid) and proposed TBD estimates (+). The horizontal dotted lines represent the boundaries of the frequency bins.

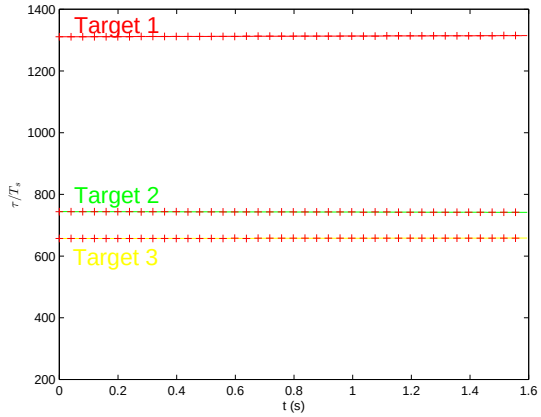

Fig. 16. Normalized bistatic delay in the maneuvering scenario: true position (solid) and batch TBD estimates (+).

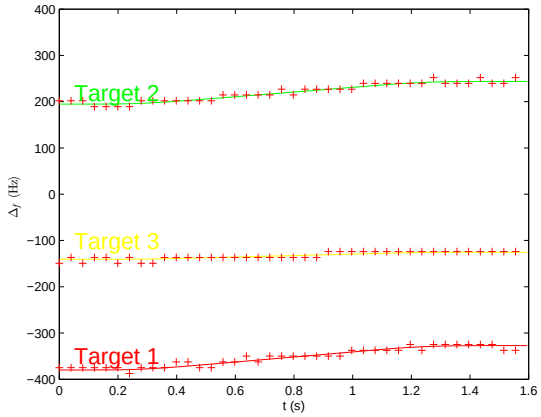

Fig. 17. Doppler shift in the maneuvering scenario: true position (solid) and batch TBD estimates (+).

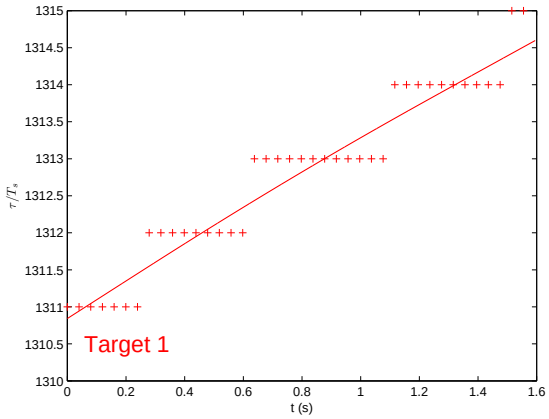

Fig. 18. Normalized bistatic delay in the maneuvering scenario for target 1: true position (solid) and batch TBD estimates (+).

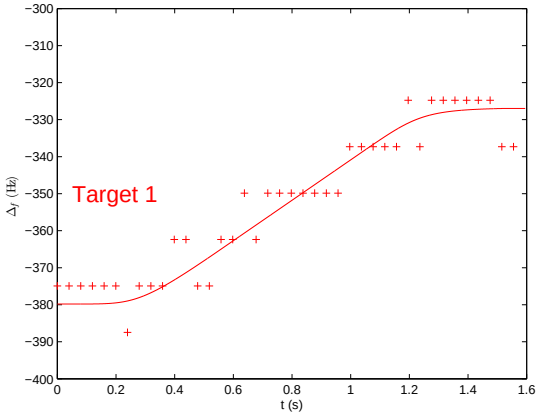

Fig. 19. Doppler shift in the maneuvering scenario for target 1: true position (solid) and batch TBD estimates (+).

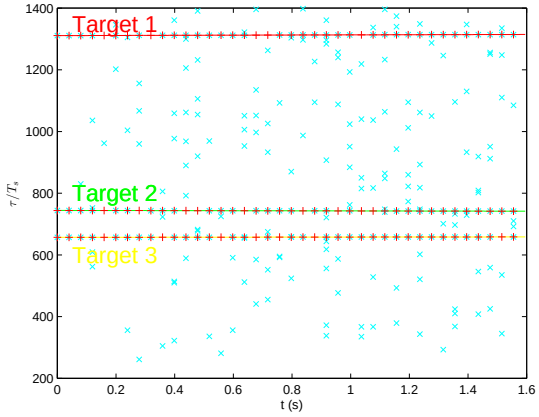

Fig. 20. Normalized bistatic delay in the maneuvering scenario: true position (solid), thresholded measurements (x) and JPDAF estimates (+).

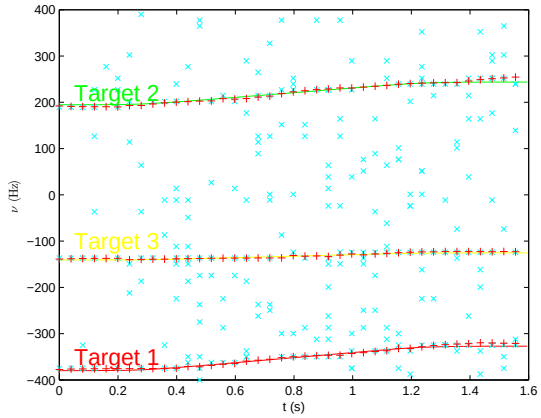

Fig. 21. Doppler shift in the maneuvering scenario: true position (solid), thresholded measurements (x) and JPDAF estimates (+).

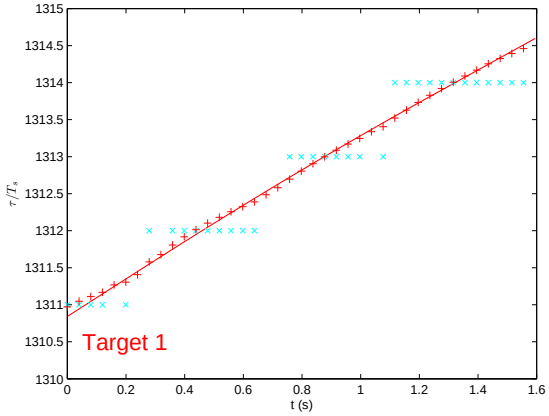

Fig. 22. Normalized bistatic delay in the maneuvering scenario for target 1: true position (solid), thresholded measurements (x) and JPDAF estimates (+).

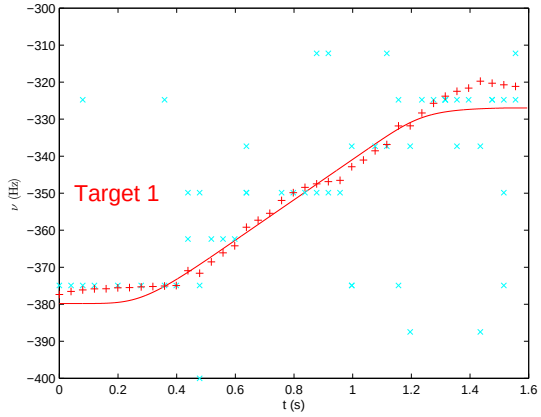

Fig. 23. Doppler shift in the maneuvering scenario for target 1: true position (solid), thresholded measurements (x) and JPDAF estimates (+).

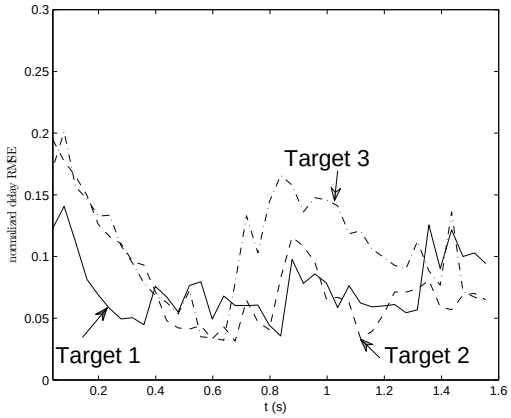

Fig. 24. Normalized bistatic delay RMSE for the TBD method in the maneuvering scenario.

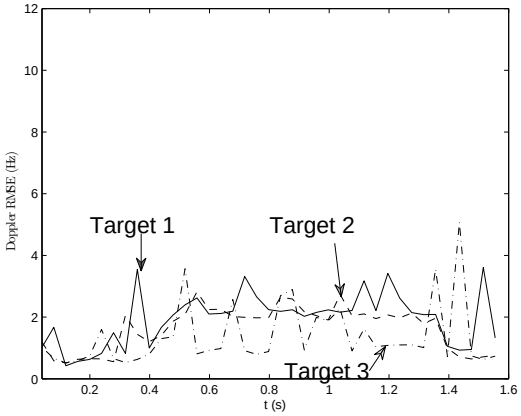

Fig. 25. Doppler shift RMSE for the TBD method in the maneuvering scenario.

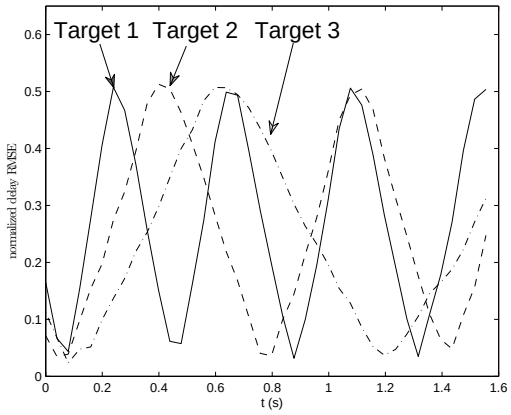

Fig. 26. Normalized bistatic delay RMSE for the batch TBD method in the maneuvering scenario.

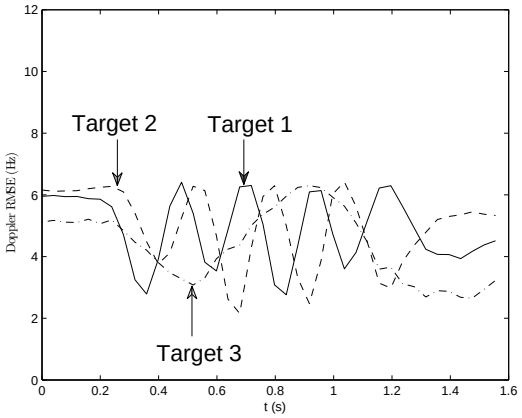

Fig. 27. Doppler shift RMSE for the batch TBD method in the maneuvering scenario.

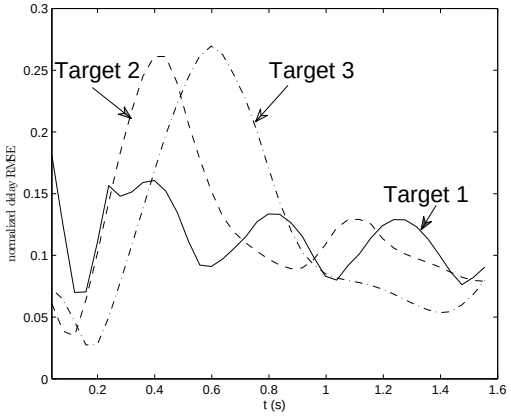

Fig. 28. Normalized bistatic delay RMSE for the JPDAF method in the maneuvering scenario.

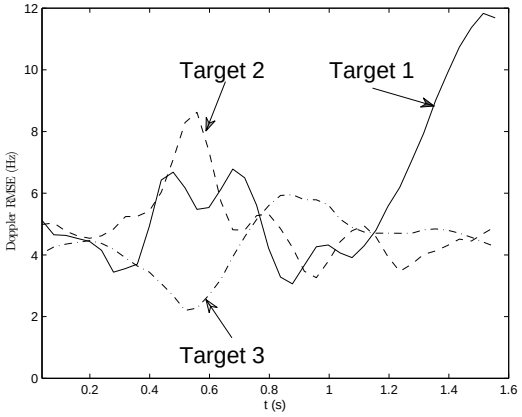

Fig. 29. Doppler shift RMSE for the JPDAF method in the maneuvering scenario.